# Underpinning wheat physiological and molecular responses to co-occurring iron and 1 phosphate deficiency stress 2

Gazaldeep Kaur, Vishnu Shukla, Varsha Meena, Anil Kumar, Jagtar Singh, Kaitheri Kandoth, Shrikant Mantri, Hatem Raouched, Ajay Kumar Pandey

1 **Underpinning wheat physiological and molecular responses to co-occurring iron and**

2 **phosphate deficiency stress**

3 Gazaldeep Kaur[1,2*], Vishnu Shukla[1*], Varsha Meena[1], Anil Kumar[1,2], Jagtar Singh[2], Pramod

4 Kaitheri Kandoth[1], Shrikant Mantri[1], Hatem Raouched[3,4,5], and Ajay Kumar Pandey[1#]

5

6 Author affiliations

7 [1]National Agri-Food Biotechnology Institute (Department of Biotechnology), Sector 81,

8 Knowledge City, Mohali-140306, Punjab, India.

9 [2] Department of Biotechnology, Panjab University, Punjab, India.

10 [3]BPMP, Université de Montpellier, INRA, CNRS, Montpellier SupAgro, 34060

11 Montpellier, France.

12 [4]Department of Plant, Soil, and Microbial Sciences, Michigan State University, East Lansing,
13 MI 48824

14 [5]Plant Resilience Institute, Michigan State University, East Lansing, MI 48824
15

16 [*]Both the authors contributed equally

17

18 [#]*Corresponding author*

19 Dr. Ajay K Pandey, Scientist-E.

20 National Agri-Food Biotechnology Institute (Department of Biotechnology), Sector 81,

21 Knowledge City, Mohali-140306, Punjab, India.

22 Telephone:     +91-1724990124

23 Email:          pandeyak@nabi.res.in; pandeyak1974@gmail.com

24 ORCID iD: https://orcid.org/0000-0003-1064-139X

25

26

27

28

29

30

31

32

33

**ABSTRACT**

Iron (Fe) and phosphate (P) are essential mineral nutrients for plant growth and development. While it is known that Fe and P pathways interacts within plants however, our understanding of the molecular mechanisms regulating nutrient interaction during plant vegetative and reproductive stages remains largely unknown. Herein, we provide a comprehensive physiological and molecular analysis of hexaploid wheat response to single P/Fe and combined Fe and P deficiency. Our data showed that wheat primary root growth was inhibited in response to –Fe, and remarkably rescued by co-occurring deficiencies of Fe and P. Transcriptome analysis revealed drastic and distinct molecular rearrangements to adapt the single and combined nutrient stress with dominance of Fe responsive cis-regulatory elements. Gene-based clustering and root-specific transcriptome expression analysis identify several important unique components induced in response to combined stress –Fe–P, including UDP-glycosyltransferases and cytochrome-P450 and glutathione metabolism. These data are consistent with our metabolome data, which further reveals specific metabolite accumulation in –Fe–P those include amino-isobutyric acid, arabinonic acid and aconitic acid. Finally, at reproductive stage alleviations of the negative effect of Fe was also observed in –Fe–P (i.e. spikelet and grain development). Collectively, the data obtained is essential for designing new strategies to improve resilience of crops to cope with the limited nutrients in soils.

**Keywords:** iron, phosphate, *Triticum aestivum*, nutrient homeostasis, growth, transcriptome.

**Highlight:** Hexaploid wheat showed distinct physiological and molecular changes during single and combined deficiency of iron and phosphate. Alleviations of the negative effect of -Fe was observed in –Fe–P combined deficiency in the root phenotype and spike development.

2

68

69 **INTRODUCTION**

70 Nutrient deficiencies in plants severely reduce the crop yields and subsequently affect the

71 worldwide nutrient balance (Marschner, 1995). Fe is an essential microelement for plant

72 growth and development, utilized in nearly every cellular process ranging from

73 photosynthesis to respiration. In general, deficiency of iron (Fe), especially in alkaline

74 calcareous soil considered as one of the most critical limitations in cereal crop production

75 (Ma and Ling, 2009; Abadia *et al.*, 2011). The rhizospheric region of the plants, including its

76 composition, pH and oxidation state influences the Fe availability and its uptake mechanism

77 by the roots (Morrissey and Guerinot, 2009) . To overcome Fe-deficiency, plants have

78 evolved tightly controlled adaptive mechanisms, which involves the developmental response

79 of root system to maximize Fe acquisition from the soil. Plants recruit two modes of

80 strategies to transport Fe, strategy I, which is a reduction-based strategy found in non-

81 graminaceous plants and strategy II which is chelation-based strategy found in graminaceous

82 species. Strategy I, involves the lowering of the pH of the rhizosphere via excretion of

83 protons, resulting in reduction of ferric chelate of the root surface and absorption of ferrous

84 ions across the root plasma membrane (Kobayashi and Nishizawa, 2012). Ferric ($Fe^{3+}$) is the

85 major abundant form in rhizosphere, which is the insoluble form of iron and cannot be taken

86 up by the plants. In contrast during the strategy II, the uptake of Fe relies mainly on the

87 biosynthesis and secretion of phytosiderophores (PS), such as mugineic acids (MAs). These

88 biochemicals make Fe-PS complexes that are subsequently transported into the roots by

89 yellow stripe like transporter proteins (YSL) (Curie *et al.*, 2001; Murata *et al.*, 2006; Inoue *et*

90 *al.*, 2009; Lee *et al.*, 2009; Nozoye *et al.*, 2011; Kobayashi and Nishizawa, 2012). The

91 molecular players involved in efflux of MA are now characterized in rice barley and very

92 recently identified in wheat (Nozoye *et al.*, 2011; Kaur *et al.*, 2019).This raises the question

93 about the extent to which the regulation of Fe homeostasis in monocots (cereals) depends on

94 the availability of other nutrients.

95

96        Phosphorus (P) is an essential macronutrient for plants to complete their life cycle,

97 and its deficiency is a major limiting factor in the crop productivity (Raghothama, 1999;

98 Heuer *et al.*, 2017; Carstensen *et al.*, 2018). Different crops recruit adaptive physiological

99 and molecular changes to acclimatize to P-deficiency (Rouached *et al.*, 2010; Secco *et al.*,

100 2017). The P-deficiency response results in multiple root developmental changes to enhance

101 its acquisition along with the changed expression profiles of important genes involved in Pi

102    transport and distribution (Misson *et al.*, 2005; Bouain *et al.*, 2016). Based on the functional

103    characterization in model plant *Arabidopsis* (dicots) and in rice (monocots), key players

104    known to be involved in P starvation are transcription factor PHOSPHATE STARVATION

105    RESPONSE (*PHR1*), microRNA399 (miR399)*,* PHOSPHATE1 (*PHO1*) and ubiquitin E2

106    conjugase (*PHO2*) (Cai *et al.*, 2012; Oono *et al.*, 2013; Secco *et al.*, 2013). Root architecture

107    changes are also reported in response to Pi deficiency (Svistoonoff *et al.*, 2007).  For

108    instance, in *Arabidopsis* the elongation of the primary root is inhibited under low P (Ward *et*

109    *al.*, 2008*b*). Key genes involved in this process were discovered including *LPR1 (*LOW

110    PHOSPHATE RESPONSE 1) (), *LPR2*, and PHOSPHATE DEFICIENCY RESPONSE

111    2 (*PDR2*) those are involved in local Pi sensing at the root tip level (Naumann *et al.*, 2019).

112    Roots tips are an active site for Pi sensing that is shown to be mediated by SENSITIVE TO

113    PROTON RHIZOTOXICITY (*STOP1*) and ALUMINUM ACTIVATED MALATE

114    TRANSPORTER 1 (*ALMT1*) resulting in the accumulation of the apoplastic Fe mediated by

115    malate (Mora-Macías *et al.*, 2017; Zhou *et al.*, 2020). This suggests that to cope the nutrient

116    stress, roots also undergo metabolic reprogramming.

117

118         Besides *Arabidopsis*, most of monocot plants including maize, rice and wheat showed

119    no reduction or slight elongation of primary roots under P-deficiency (Narayanan, A. Reddy,

120    1982; Mollier and Pellerin, 1999; Shimizu *et al.*, 2004).While in *Arabidopsis* the primary root

121    inhibition was proposed to be partly due to Fe toxicity at root tip (Ward *et al.*, 2008*b*), no Fe

122    toxicity is reported in cereal crops grown under P deficient condition. Thus the overall

123    performance of the plants depends on the Pi availability and its interaction in the complex

124    rhizospheric area with Fe and other metals (Bouain *et al.*, 2014; Xie *et al.*, 2019). So how

125    monocots (cereals) coordinate P and Fe remains largely unknown.

126

127         Given to their opposite charge, Fe (II) is known to readily interact with inorganic

128    phosphate ($HPO_3$-, Pi) in the soil or growth medium, near root surface and within the plant.

129    When both Pi and Fe are absorbed at the same time, availability of both the nutrients gets

130    affected due to precipitation (Dalton *et al.*, 1983). Multiple studies have provided the

131    preliminary clue for the probable interaction of P with the absorption of important

132    micronutrients like iron (Fe) (Chutia *et al.*, 2019; Xie *et al.*, 2019). It has been reported that

133    under P-deficiency, reduced expression of Fe homeostasis related genes could be due to

134    enhanced Fe availability to the roots under low P (Hirsch *et al.*, 2006; Ward *et al.*, 2008*b*).

135    Although, downregulation of Fe-homeostasis specific genes was observed during P-

136    deficiency, the physiological and molecular effects during combinatorial lowering of P and

137    Fe remain obscure.

138

139         Wheat is an important crop and is the major source of nutrition. Studying the

140    molecular attributes of Fe and P crosstalk will help in designing a suitable model to optimize

141    crop productivity during nutrient deficiency. Nevertheless, to date, despite its primary

142    interest, a molecular event recruited by wheat to cope with P and Fe combined stress still

143    waits examination. In the current study we performed a comprehensive analysis of

144    physiological, transcriptional and metabolic changes in hexaploid wheat under single –Fe and

145    –P and combinatorial deficiencies of Fe and P (–Fe–P). Special focus was laid to dissect the

146    underlying molecular events  in crosstalk of Fe and Pi during plant growth till their seed

147    production, by combining transcriptomic and metabolomic approaches. An important role of

148    genes involved in strategy II mode of Fe uptake under contrasting regimes of P was observed.

149    Distinct transcriptional and metabolic regulation was observed in the roots of wheat during –

150    Fe–Pi response. Knowledge gained in this study expands our understanding of how cereal

151    crops respond to multiple simultaneous nutrient stress and how those are coordinated at the

152    whole plant level.

153

154    **MATERIALS AND METHODS**

155    **Plant materials**

156    A bread wheat variety 'C-306' was adopted and grown hydroponically under the Hogland's

157    nutrient solution containing ($L^{-1}$): 6 mM $KNO_3$, 1mM $MgSO_4.7H_2O$, 2 mM $Ca(NO_3).4H_2O$,

158    200 µM $KH_2PO_4$, 20 µM Fe (III) EDTA, 0.25 mM $H_3BO_3$, 0.002 mM $MnSO_4.H_2O$, 0.002

159    mM $ZnSO_4.7H_2O$, 0.0005 mM $CuSO_4.5H_2O$, 0.0005 mM $Na_2.MoO_4$ and 0.05 mM KCL. After

160    overnight stratification at 4°C, wheat seeds were germinated for 5 days in distilled water.

161    Once the endosperm starts browning it is removed from the developing seedlings. Seedlings

162    were then transferred to PhytaBox$^{TM}$ and grown in the nutrient solution described above.

163    After 7 days, nutrient solutions were replaced on the basis of different treatments. For +Fe–P

164    treatment, 20 µM $KH_2PO_4$ was used for P-deficiency. For –Fe+P treatment, 2 µM Fe (III)

165    EDTA was used for Fe-deficiency. While for –Fe–P treatment, 20 µM $KH_2PO_4$and 2 µM Fe

166    (III) EDTA was used for both Fe/P deficiency. For control plants (+Fe+P) concentrations of

167    nutrients were unchanged in above mentioned Hoagland's solution. After germination, plants

168    were grown in the described medium for 20 days in growth chamber set at 20□±□1□°C,

169    50–70% relative humidity and photon rate of 300□µmol quanta $m^{-2}$ $s^{-1}$ with

170    16□h□day/8□h night cycle. The whole set of experiment was repeated four times to

171    examine biological variation. For sampling, roots and shoots were collected at different time

172    points after deficiency (5d, 10d, 15d and 20d). Samples were snap frozen in liquid nitrogen

173    and stored at -80°C. On the basis of distinct phenotype samples collected at 20 days after

174    deficiency (DAT) were used for further analysis. To distinctively observe primary root and

175    1st order lateral root, individual plants were moved onto a 150mm wide petriplate filled with

176    distilled water and characteristics was manually examined. Eight biologicals replicated for

177    each above-mentioned treatment were used to ascertain root characteristics.

178

179        For the prolonged iron and phosphate deficiency individual seedlings were transferred

180    into respective pots filled with soilrite (5 seedlings each) in three replicates manner and

181    allowed to grow in growth chamber set at 20 ± 1 °C, 50-70% relative humidity and photon

182    rate of 300µmol photons m$^{-2}$ with 16h day/8h night cycle. Pots were watered with Hogland

183    medium solution with the condition as mentioned above twice a week. The main individual

184    spikes of the each replicate were tagged at the first day after anthesis (DAA). Total of 15

185    plants were sampled for each condition. After the maturation of the plants (55 days), spike

186    tissues (rachis, glumes, awn and seeds) were harvested and images were processed. For

187    comparing morphological differences, length and total weight of matured spike tissues from

188    each condition was measured.

189

190    **RNASeq experiment design and sequencing**

191    Wheat 20 days old root tissue samples for the four conditions (+Fe+P, +Fe–P, –Fe+P and –

192    Fe–P) with at least two to three biological replicates derived from at least two independent

193    RNA extractions were pooled together. Each of biological replicates consists of 12-15

194    seedlings per treatment. Samples were collected at the same time, snap frozen in liquid

195    nitrogen and stored at -80°C. The RNA extraction as well as Illumina sequencing was

196    performed for two biological replicates for –P and three for –Fe–P with their respective

197    controls. For Fe-deficiency. previously published RNAseq datasets were used (Kaur *et al.*,

198    2019). RNA extraction for library construction from the control and treated root samples was

199    performed as reported earlier (Kaur *et al.*, 2019). Briefly, sequence libraries were prepared

200    from high quality, quality control passed RNA samples using Illumina TruSeq mRNA library

201    prep kit as per the instructions (Illumina Inc., USA). The reads were sequenced using 2 X 150

202    bp chemistry on NextSeq 500 and NovaSeq6000.

203

6

**Sample clustering and differential expression analysis**

Paired-end reads were quality trimmed and adapter filtered using Trimmomatic v0.35 to retain only good quality reads (QV>20). The clean raw reads were quantified for expression by pseudoalignment against wheat transcriptome (ensembl release 46) using Kallisto v0.44.0 (Bray et al., 2016), using the option --rf-stranded for stranded samples. DESeq2 R package (Love *et al.*, 2014) was used for differential expression analysis. Raw counts values from Kallisto were summarized from transcript to gene level abundances and imported for use with DESeq2 using tximport package (Soneson *et al.*, 2015). Principal Component analysis (PCA) was performed based on VST transformed counts for all samples to observe clustering across replicates and conditions. The samples from batches were taken together to build a DESeq2 model to obtain normalised counts, which were transformed using VST mode and corrected for the associated batch effect using remove Batch Effect function from limma package (Ritchie *et al.*, 2015). ggplot2 package (Wickham, 2017) was used to design the PCA plot. Clustered heatmap for selected 500 genes with highest variation in expression among the conditions was generated using pheatmap package.

For differential expression analysis, DESeq() function was used to calculate the relative expression for the pairwise comparisons among conditions. Log2 Fold Changes (LFC) were obtained for the pairwise comparisons for each of the three deficiency conditions w.r.t. control (+Fe+P) from the respective batch group only, so as to avoid any variation due to batch effects. The relative expression ratios were shrunk using apeglm package (Zhu *et al.*, 2018) to adjust the LFC of genes with extremely low counts.

**Functional enrichment analysis and annotation**

KOBAS (KEGG Orthology-Based Annotation System) standalone tool was used to firstly annotate wheat genes based on blast mapping against rice RefSeq and RAP-DB sequences, e-value <$10^{-5}$. For pathway enrichment analysis, identify module was used to shortlist the significantly overrepresented KEGG pathways for the respective deficiency conditions using Fisher's exact test. FDR correction was performed using Benjamini and Hochberg method. Also, MapMan (Thimm et al., 2004) was used to map the DEGs onto metabolic, regulatory and other biological categorical pathways. The mapping file was generated through Mercator (Lohse et al., 2013), using the wheat transcriptome fasta file as an input. In addition, wheat RefSeq v1.1 annotation released by International Wheat Genome Sequencing Consortium (IWGSC) was also used (https://urgi.versailles.inra.fr/download/iwgsc).

7

238

**Identification of cis-regulatory elements**

To check the extent of Fe or P specific transcriptional regulation in –Fe, –P as well as combined deficiency of –Fe–P, 2000 bp upstream promoter region sequences for the three sets of DEGs were downloaded from Ensembl Biomart. The promoter sequences were checked for presence of 115 frequent cis-regulatory elements (freq-CREs) enriched in clusters for gold standard (GS) Fe responsive genes (Schwarz et al., 2020) and phosphate regulation specific CREs using an in-house perl script (link). For validation and comparison, three sets of control groups with 100 promoters each were randomly shortlisted from genes that were not altered in response to Fe-deficiency (-0.5 > LFC < -0.5).

**Gas chromatography–mass spectrometry metabolite profiling**

Extraction of total metabolites was performed similarly as previously described (Wang et al., 2018; Kaur et al., 2019). Wheat roots subjected to +Fe+P, +Fe–P, –P +Fe and –Fe–P were sampled at 20 days after deficiency in triplicate manner and processed for metabolite extraction. The derivatized metabolites were analysed with a GC instrument (Agilent technologies 7890, USA) coupled with mass spectrometry. Measurement from an injection volume of 1 µl was taken in split-less mode in DB-5 column (30 m × 0.25 mm, 0.25 µm film thickness, Agilent) using helium as carrier gas. For analysis, qualitative analysis of chromatograms was performed in MassHunter Qualitative analysis Sp1 workstation (Agilent, USA). Identification and annotation of each compound was supervised manually using AMDIS software and NIST08 database (http://www.nist.gov/srd/mslist.html). Data were normalized to sample weight and internal control (sorbitol). Statistical analysis was performed as described earlier (Quanbeck *et al.*, 2012). Log2 ratio of metabolite abundances in tested conditions was plotted against control condition (+Fe +P). Delta method approximation was used to calculate standard errors (se) of log-ratio, se log-ratio = $1/\ln 2\sqrt{[(SE_T/T)^2 + (SE_C/C)^2]}$, where $SE_T$ and $SE_C$ are standard errors of average test and control metabolite abundances. For PCA and hierarchical clustering analysis, clustvis (https://biit.cs.ut.ee/clustvis/) online program package with Euclidean distance as the similarity measure and hierarchical clustering with complete linkage was used. A tab-delimited file was used as input comprising of annotated metabolites with their corresponding log transformed concentration values in triplicates for each condition.

**Quantitative real time-PCR (qPCR) analysis**

8

272    Total RNA was isolated from the roots of the 20 DAT (days after treatment) seedlings. A

273    total of 2ug of RNA was used to prepare cDNA by using SuperScript III First-Strand

274    Synthesis System (Invitrogen, USA). For removing the genomic contamination in the RNA

275    sample, they were pre-treated with TURBO DNA-free kit (Ambion, TX, USA). To perform

276    quantitative RT- PCR (qRT-PCR) amplification was performed using gene specific primers

277    (Table S1) along with internal control ARF (ADP-Ribosylation Factor) to normalize the

278    expression data for each gene by the using of Ct method [$2^{(-\Delta\Delta Ct)}$] in the CFX96$^{TM}$ Real-Time

279    PCR System (BioRad Inc, USA). Two or three independent replicates with four technical

280    replicates were performed for each sample. The relative amount of gene expression was

281    calculated by $2^{-\Delta\Delta CT}$ method (Livak and Schmittgen, 2001) for every cDNA samples.

282

283    **Metal analysis in wheat tissues, Perl staining and root Fe mobilization assay**

284    Seed phosphorus and different metal analysis was performed using Inductive Coupled

285    Plasma-MS (ICP-MS). Metal analysis was performed as described previously (Bhati *et al.*,

286    2016; Aggarwal *et al.*, 2018). Briefly, the mature seeds were grounded to fine powder and

287    subsequently subjected to the microwave-digested with $HNO_3$ (SuraPure$^{TM}$, Merck).

288    Respective metal standards were also prepared for analysis. Three independent replicates

289    were performed for each 20 DAT samples. For Perl staining, wheat roots were incubated with

290    Perl's Prussian blue (PPB) method consisting of with equal amount of premixed solution of

291    4% (v/v) HCL and 4% (w/v) Potassium hexacyanoferrate (II) trihydrate. Roots of eight to ten

292    wheat seedlings from each experiment were taken and incubated in above solution mixture

293    for 30 mins. Blue colour Fe-plaques were observed for the presence of Fe on the wheat roots

294    seedlings and representative images (five seedlings per treatments) were taken for respective

295    treatments. To estimate the PS release, Fe remobilization assays of wheat roots was

296    performed in aerobic condition as described earlier in detail (Takagi, 1976; Kaur *et al.*,

297    2019). For PS release twenty-five wheat seedlings undergoing the respective treatments were

298    used for release in 60 ml deionised water in presence of Micropur (Katadyn, Switzerland).

299    The final concentration of the released ferrous ion was estimated by measuring OD at 562

300    nm.

301

302    **Statistical data analysis and data availability**

303    To identify significant differentially expressed genes, a cut-off criterion of LFC > 1 in either

304    direction, with an adjusted p-value (padj) of less than 0.05 was set. The padj values were

305    obtained by using the Benjamini and Hochberg approach for controlling the false discovery

9

306     rate. The RNAseq data generated in this study has been deposited under the NCBI SRA

307     database BioProjectID (submission pending).

308

309     **RESULTS**

310

311     **Fe and P interplay to regulates Fe uptake.**

312     Wheat responses to either Fe or P deficiency are fairly documented at physiological and

313     molecular level (Oono *et al.*, 2013; Kaur *et al.*, 2019). But little information is available on

314     how wheat integrates simultaneous Fe and P stress and how wheat adjusts it growth capacity

315     accordingly. Therefore, we compared wheat growth under four growth conditions, namely

316     nutrient-sufficient (+Fe+P), single nutrient deficiency (–Fe+P, +Fe–P), and combined

317     nutrient deficiency (–Fe–P). Short (5 days post treatment, dpt), medium (10 dpt) and long-

318     term (20 dpt) effects of these nutritional growth conditions on wheat morphology and

319     biomass allocation pattern were assessed. At all the time points, Fe-deficient plants displayed

320     shorter roots compared not only to control (+Fe+P) plants but also to plants grown on –P and

321     –Fe–P conditions (Figure 1A & B). The primary root length significantly increased during –P

322     condition. Interestingly, combined Fe and P (–Fe–P) lead to the recovery of total primary root

323     elongation, thus alleviating the negative effect of Fe-deficiency (Figure 1C). Similar trend

324     was also observed for the number and length of the 1$^{st}$ order lateral roots which shows

325     significant increase during –P and –Fe–P conditions compared to just Fe-deficient and

326     control plants (Figure 1D and E). Examination of the fresh biomass allocation patterns from

327     shoot to root was assessed as well. The total plant biomass was higher in control seedlings

328     (~1.7 grams) and lowest in –Fe–P condition (~0.6 grams) (Figure 1F). While, wheat roots

329     under –Fe showed very low allocation of root and the allocation pattern of biomass in –P and

330     –Fe–P plants were similar (Figure 1F).  Collectively our data suggests that Fe and P crosstalk

331     and thereby are able to regulate the root characteristic.

332

333         The availability of P or Fe was shown to influence the uptake of Fe or P respectively,

334     and perhaps better characterized in *Arabidopsis* (Ward *et al.*, 2008*a*). Nevertheless, this key

335     step for P and Fe in wheat is not well studied. To test the effect of P or Fe availability on P or

336     Fe uptake ICP-MS analysis, Pi uptake, Perl's staining (for Fe) of the roots were performed.

337     As expected, the accumulation of Pi was reduced either in –P or –Fe–P treatments. In our 20

338     dpt roots, Fe-deficiency does not influence Pi uptake under single –Fe+P deficiency (Figure

339     2A). In contrast, ICP-MS analysis revealed that only during P-deficiency conditions

340    significant increase in the accumulation of Fe in the roots was observed compared other

341    treatments (Figure 2B). In addition to this, wheat roots showed higher Zn accumulation under

342    –Fe–P and Mn in +Fe–P condition (Figure 2B). In shoots, only Mn was accumulated in

343    higher amount during –Fe–P. Perl's staining analysis showed no visual presence of Fe in

344    roots under –Fe and –Fe–P conditions (Figure 2C). Enhanced Fe-plaque colorization under –

345    P conditions and mild staining in +Fe+P roots was observed (Figure 2C). This suggests that

346    Fe is aggressively taken up by the plant roots under –P conditions. A key aspect of Fe uptake

347    in cereals is the release of PS for Fe remobilization (Römheld and Marschner, 1986;

348    Römheld, 1991). Accordingly, our assays revealed a high release (42-47 nM) of PS under –

349    Fe condition (10 dpt) (Figure 2D). While, the PS release decreased during –Fe–P condition

350    (16-18 nM) compared to –Fe conditions, significantly higher compared to –P (8-9 nM) and

351    controls (2-3 nM) conditions (Figure 2D). This data indicates that the presence of P is

352    necessary for the wheat roots to respond to Fe deprivation so as to enhance the release of PS.

353

354    **Comparative analysis of normalized RNAseq expression**

355    Nutrient deficiency alters plant transcriptomes. We recently showed that Fe deprivation

356    results in important global gene expression reprogramming in wheat (Kaur *et al.*, 2019). But

357    how combined Fe and P influence transcriptome remains unknown. Therefore, we set out to

358    gain insight of the transcriptional responseupon combined Fe and P deficiency stress (20 dpt)

359    through RNAseq. In all, 240,013,343 million quality filtered reads with 89% reads having

360    quality score >= Q30 were used for the differential expression analysis using the Kallisto-

361    DESeq2 pipeline (Bray et al., 2016; Love et al., 2014). In response to –P condition, 2983 and

362    802 genes were downregulated and upregulated respectively (Figure 3A, Table S2). Fe–P

363    combined stress cause an upregulation and downregulation of 1829 genes and 951 genes

364    respectively (Table S2). Refined analysis of our previous –Fe transcriptome subsequently

365    identified 2055 up- and 2191 downregulated genes as –Fe response w.r.t. control (Figure 3A)

366    (Kaur *et al.*, 2019), the Venn diagram revealed those genes that are unique or commonly

367    regulated by Fe and P (Figure 3B and Table S3, S4). Finally, clustered heatmap analysis of

368    all 4 transcriptomes revealed that the transcriptome of control and –Fe–P plants were closer,

369    and distant from those of single Fe or P deficiency conditions (Figure S1A & B).

370    Furthermore, clustered heatmap analysis of the top upregulated genes (top 100 genes) across

371    all treatments suggested that expression of these genes was similar in –Fe and –Fe–P

372    conditions (Figure 3C). In contrast, most of the strongly downregulated genes (left panel)

373  showed similar patterns during –Fe and –P. This suggest that wheat roots respond to dual

374  deficiency of Fe and P.

375

376  **Specific and overlapping genes regulated by Fe and/or P deficiency in wheat roots**

377  Under the P-deficiency, wheat induces genes for key transcription factors (Table S5)

378  including PHOSPHATE STARVATION RESPONSE (PHR) homologs and its targets such

379  as PHO1;H1, TaIPS1. Phosphatase related genes like phosphate starvation-induced gene 2

380  (PS2) were induced, whereas downregulation of PURPLE ACID PHOSPHATASE (PAP)

381  and UDP-GLYCOSYLTRANSFERASES genes was noted (Table S2). Additionally, SPX

382  domain genes also showed induced expression. Our analysis confirmed the P-deficiency

383  response in wheat roots. In contrast, 8 genes encoding for UDP-

384  GLYCOSYLTRANSFERASE were induced during –Fe–P. Glutathione S-transferase, NBS-

385  LRR family, chaperone related genes, ABC and ion transporters were also highly expressed

386  in response to –Fe–P. Additionally, three putative nitrate transporters-NRT

387  (TraesCS5A02G388000; TraesCS7A02G428500; TraesCS3B02G285900) and a gene

388  encoding for nitrate reductase were remarkably downregulated. These expression responses

389  marked the characteristic–Fe–P response in wheat roots along with the downregulation of

390  stress responsive genes including hydrolase and ATP binding proteins (Table S2).

391  Phytohormone genes such as auxin pathway and including PIN and IAA sub-family genes

392  were significantly expressed in –Fe–P (Figure 4A, Table S6). Overall, our data indicates that

393  auxin biosynthesis and secondary metabolism genes for lignification were highly active in the

394  –Fe–P that could support the root phenotype (Figure S2). Interestingly, the overlapping

395  response of transcripts altered during –P and –Fe–P was found to be very low (15.79%), and

396  included multiple PSR responsive/regulated genes (Figure 4B, Table S7). Total of 39 genes

397  were commonly upregulated specifically by –P and –Fe–P. Genes encoding for Glycine-rich

398  cell wall structural proteins were highly upregulated in both conditions (Table S8). In

399  contrast, 110 genes were commonly downregulated during these two conditions. Among the

400  common list peroxidase and proteases were highly repressed. 206 genes showed contrasting

401  expression in –P and –Fe–P, with number of germin-like protein encoding transcripts, and

402  GDSL esterase, CytP450, Glutathione S-Transferase and ABC transporters (Table S8).

403

404  Interestingly, the overlapping response of transcripts specifically during –Fe and –Fe–

405  P was found to be comparatively high (24.96%). Comparative –Fe (Kaur *et al.*, 2019) and –

406  Fe–P transcriptome analysis revealed that 83.65% of–Fe alone DEGs were no longer

12

407    differentially expressed under the combined –Fe–P treatment (Figure 4C). This suggests that

408    plant use reprogrammed pathways to respond in dual nutrient deficiency as compared to

409    response during single deficiency stress. In total, 494 genes were coregulated irrespective of

410    presence or absence of P, among these 84 genes were observed to be significantly altered in

411    all three deficiency conditions. While 410 genes were commonly regulated by Fe-deficiency,

412    either upregulated (i.e. nicotianamine synthase genes-NAS, basic helix loop helix-bHLH and

413    WRKY transcription factors, and transporters viz., ZIFL, YSL, NRT1) or repressed (i.e.

414    ABC-G family peroxidases, arabinogalactan protein encoding, sulfate transporter, ferritin and

415    loricrin like genes) regardless of P status in the growth medium. 200 genes showed opposite

416    expression pattern mainly including no apical-meristem (NAC) domain containing, cobalt-

417    ion protein encoding , glycosyltransferases and zinc transporter genes were marked by this

418    category (Table S9).

419

420         During –Fe or in –Fe–P, multiple genes involved in Fe homeostasis were induced

421    suggesting that presence of P does influence the expression of Fe related genes. Furthermore,

422    93 Fe starvation responsive genes (FSR; Strategy I and II) were checked for their expression

423    response (Table S7). Most of the FSR genes showed downregulation in P-deficiency, but

424    were upregulated either in –Fe+P or –Fe–P (Figure 4D). Up-regulated genes also included

425    those involved in biosynthesis of PS *via* methionine cycle.  Lastly, 84 genes were commonly

426    altered in all three growth conditions i.e. +Fe–P, –F+P and –Fe–P (Table S9).  Only one

427    fourth of these genes were significantly commonly upregulated such as WRKY transcription

428    factor and genes encoding SPX domain containing protein. 62 genes were downregulated

429    including ABC-G family, and TaYSL12 encoding genes.

430

431    **KEGG pathway enrichment analysis of DEGs and metabolome analysis**

432    Mapman based analysis suggest that high expression of genes involved in UDP-glycosyl-

433    transferases and GST related pathways during –Fe–P, when compared to other treatments and

434    controls (Figure 5A). Overall, our data indicates that auxin biosynthesis and secondary

435    metabolism genes for lignification were highly active in –Fe–P response (Figure S2, S4). To

436    further categorise the DEGs from each nutritional growth conditions in their corresponding

437    metabolic pathways we mapped them to the KEGG database. Our analysis revealed that in

438    response to P-deficiency (+Fe–P), genes related to phenylpropanoid pathway, photosynthesis,

439    ABC transporters, and genes for nitrogen metabolism were highly enriched (Figure 5B). In

440    response to –Fe–P conditions, enrichment of genes involved in glutathione metabolism,

441 glycerophospholipid metabolism, starch and sucrose metabolism and galactose metabolism

442 pathways and cysteine and methionine metabolism was observed (Figure 5B). Interestingly,

443 enrichment of cysteine and methionine metabolism genes was also observed in response to –

444 Fe+P treatment (Kaur *et al.*, 2019), indicating that the enrichment of genes is Fe specific, and

445 independent of P status.

446

447 To further study the role of primary metabolites during the Fe and P interaction GC-

448 MS analysis was done using the fresh roots of the wheat seedlings post 20 dpt. Our analysis

449 showed that significant variation in the accumulation of metabolites between nutrient-

450 deficient and nutrient-sufficient plants along with a variation amongst nutrient deficiency

451 treatments (Figure 6A, Table S10). While suppression of oxalic acid and increase in 4-

452 ketoglucose levels was unique for –P treatment, the increase in fumaric acid and myo-inositol

453 marked metabolic change was specific for –Fe conditions. A contrasting level of serine and

454 succinic acid in +Fe–P (low) and –Fe+P (high) was found to be normalized in dual deficiency

455 with respect to control. The –Fe–P conditions is characterized by specific metabolic changes

456 marked by decrease in acetic acid, butanoic acid, valine, threonine and glucofuranoside levels

457 and increased accumulation of β-amino-isobutyric acid, strearic acid, arabinonic acid and

458 aconitic acid. Nevertheless, numerous metabolitesdecreased commonly in –Fe–P and –Fe

459 conditions such as aspartic acid, hexonic acid, glucose cystathione and, alanine. While the

460 acids showed high accumulation in –Fe they were highly reduced during –Fe–P. The

461 metabolites that decrease in –Fe–P appeared to follow the same trends in –P conditions

462 including citric acid and hexapyranose. Finally, sugars,sugar conjugates (i.e. d-ribofuranose,

463 a-d-galactopyranoside, a-d-mannopyranoside), amino acids (i.e. b-aminoisobutyric acid,

464 cystathione and L-alanine),aconitic acid and arabinonic were predominant in –Fe–P

465 conditions (Figure 6B).

466

467 **Enrichment of Fe responsive cis-regulatory elements in regulated genes**

468 To get an insight into the regulatory function of the expressed genes during single (–Fe, –P)

469 and combined (–Fe–P) nutrient stress, Fe responsive cis-regulatory elements were analysed.

470 Our analysis revealed multiple TFs that are predominantly expressed in -Fe-P condition as

471 compared to P-deficiency (Table S5, Figure S5). Especially, genes encoding for multiple

472 bHLH, C2H2 and NAC TFs were highly represented in –Fe–P. Earlier the comprehensive

473 resource of new putative frequent cis-regulatory elements (freq-pCREs) were identified in the

474 gene clusters responsive for Fe-deficiency in roots (Ivanov *et al.*, 2012; Schwarz *et al.*, 2020).

14

475    Herein we included genes differentially regulated in response to the deficiency of Fe and/or

476    P. To optimize and validate our analysis, we used three control sets of genes (~100) with

477    log2FC between -0.5 and 0.5 in –Fe w.r.t to control and checked for the occurrence of freq-

478    pCREs in their promoters. All the random sets behaved in a similar pattern with low presence

479    of these elements (Table S11). Our analysis identified that differentially accumulated

480    transcripts are enriched with the uniform percentage distribution of freq-pCREs. To address

481    the mechanistic understanding of Fe responsive freq-CREs, analysis wasdone in subset of

482    FSR genes and PSR genes. Interestingly, when FSR and PSR related genes were analysed

483    this balance was found to be perturbed. The dominance and biasness of freq-pCREs was

484    observed significantly in Fe deficiency (Table 1). For example, cis-domains such as AAGTA,

485    ACTAGT, CACACG, AATTGC and CGTGCC were present in higher proportion in Fe-

486    deficiency responsive genes as compared to P deficiency. Our work revealed an overlapping

487    response of DEGs during Fe and P deficiency as freq-pCREs were highly enriched in Fe-

488    deficiency and was present in the promoters of P response related genes. Similarly, cis-

489    element for phosphate responsive region such as P1BS (PHR1 binding sequences,

490    GNATATNC) was present at 62% of the PSR and 23.66% of FSR genes (Table S12).

491    Interestingly, P1BS motif was present 34.97, 34,61% and 36.91% in the promoter regions of

492    DGEs in response to –Fe+P, +Fe–P and –Fe–P respectively.

493

**Effect of prolonged Fe and P deficiency on the panicle development**

495    So far, investigation of Fe and P focused on their individual and combined effect in model

496    plants. But, how long-term Fe and/or P deficiencies affects late stage of crop is largely

497    unknown. Therefore, we assessed the physiological and molecular responses of wheat plants

498    subjected to prolonged periods and effect of Fe and P deficiency (Figure 7A). In 55 days old

499    wheat plants, Fe-deficiency causes the most severe effects on productivity, spike length, and

500    rachis development compared to other treatments (Figure 7B, C & D). Strikingly, Fe starved

501    plants showed no seed setting and this phenomenon correlated with the decrease in the length

502    of awn and rachis. The above-mentioned developmental effects were less predominant under

503    prolonged –P condition. Interestingly, the negative effect of prolonged exposure of Fe

504    deprivation on spikelet development is rescued by the –Fe–P treatment. Our result show that

505    removal of P along with Fe was able to rescue the growth retardation in spike and seed

506    development. Overall, our data suggest that the inhibitory effect caused by Fe-deficiency on

507    wheat development could be minimized by subjecting the seedlings to P deprivation.

508

15

**DISCUSSION**

509

510   Fe and P are essential elements for plants, utilized in nearly every cellular process. In crops,

511   there is limited understanding of the interaction between Fe and P homeostasis to coordinate

512   physiological and molecular response. The current work aimed to fill this knowledge gap by

513   providing first insight on wheat response to Fe and/or P deficiency stresses. Our data showed

514   that P-deficiency compensates Fe negative effect on wheat growth and development such as

515   root growth and spike development. Our transcriptome analysis suggests the enriched

516   presence of putative Fe responsive cis-regulatory binding sites. By combining transcriptome

517   and metabolome analysis, we revealed a specific component underlying during Fe and P

518   combined stress response in wheat.

519

520         To sustain the Fe or P deficiency in soil, crop plants like rice, maize and soybeans

521   have adapted multiple strategy responses so as to maximize their survival under depleted

522   soils. But how crop plant responds to co-occurring Fe and P stress remains poorly

523   understood. Our study revealed that Fe uptake is dependent on P status in the rhizospheric

524   region. The enhanced accumulation of Fe could be accounted for by the continued expression

525   of Strategy-II related genes (Figure 2D and Figure S3B). These observations are in line with

526   early work where we showed that wheat use Strategy-II genes to respond to Fe-deficiency

527   (Kaur *et al.*, 2019). Genes expressed in response to –Fe and –Fe–P reinforce thus that wheat

528   primarily uses Strategy-II mode for Fe uptake even during changing regimes of P. For

529   instance, the relatively high release of PS and gene expression patterns of certain specific

530   YSL, metal transporters and a few TFs involved in metal homeostasis either in –Fe or –Fe–P

531   confirms that wheat primarily utilizes Strategy-II mode of Fe uptake route to mobilize Fe

532   from roots to shoots even under P-deficiency (Figure S3) (Kumar *et al.*, 2019; Kaur *et al.*,

533   2019). Under P-deficiency, wheat decreases citrate levels, and increases expression of citrate

534   synthase that could subsequently favor citrate exudation and this could be one important

535   mechanism for higher Fe accumulation under P-deficiency (Table S10 and Figure 6A). On

536   the other hand, Fe-deficient wheat roots tend to accumulate high levels of citrate with

537   downregulation of citrate synthase transcript (TraesCS7A02G409800). Citrate being an

538   Fe(III) chelator has been reported to play a relevant role in iron acquisition and xylem Fe

539   transport (Durrett *et al.*, 2007; Valentinuzzi *et al.*, 2015). Our transcriptome changes support

540   these metabolic changes. Indeed, P-deficiency showed an increase in transcript abundance of

541   citrate synthase (TraesCS4A02G142400) that further supports the speculation of citrate

542   exudation. Overexpression of citrate synthase has been shown to support plant growth under

16

543    P-deficiency by increasing citrate exudation (Anoop *et al.*, 2003). Furthermore, our OMICs

544    study revealed that oxalate, fumarate and aconitate that accumulated specifically under P, Fe

545    and dual deficiency respectively suggest distinct TCA cycle programming and energy

546    balance (Igamberdiev and Kleczkowski, 2019). Our data further confirmed that plants

547    accumulate/release of organic acids, mainly malate and citrate under P and Fe deficiencies to

548    the rhizospheric regions for efficient mineralization (Kania et al., 2003; Ligaba et al., 2004;

549    Wu, Liu, Riaz, Yan, & Jiang, 2019; Zhang et al., 2015; Kania, Langlade, Martinoia, &

550    Neumann, 2003; Mimmo et al., 2014).).  The cross-talk between P and Fe to regulate Fe

551    uptake and transport has been also reported in dicots, such as *Arabidopsis*. For instance, P-

552    deficiency was shown to induce expression of Fe homeostasis related genes like AtFRO2,

553    AtIRT1 and ferritin genes (*Atfer1*) (Misson et al., 2005; Y.-H. Wang, Garvin, & Kochian,

554    2002;Bournier et al., 2013). Likewise, Fe-deficiency can induce expression of P acquisition

555    genes (Thimm *et al.*, 2004; Lucena *et al.*, 2019). These evidences along with our observations

556    reinforce a strong link between the molecular interactions between P and Fe homeostasis in

557    crops.

558

559        Identifying the specific signatures for the dual deficiency of –Fe and –P will provide

560    an important link for homeostatic interaction between micro and macronutrient interaction.

561    This study led to the identification of specific signatures at the transcript and metabolome

562    level. In plants phenylpropanoid pathway (PPP) is the source of numerous phenylalanine

563    derivatives involved in multiple development and physiological process, including lignin

564    biosynthesis and cell wall development (Douglas, 1996; Boerjan *et al.*, 2003). The role of

565    glycosyltransferases has been demonstrated to efficiently control the phenylpropanoid

566    pathway (Aksamit-Stachurska *et al.*, 2008). The high expression of UGT transcripts during –

567    Fe–P suggest reorganization of metabolic pathways that resulted in the identification of

568    molecular signatures. Our MapMan analysis reinforces this, wherein high expression was

569    observed for genes, especially encoding for simple phenols, lignin biosynthesis, isoflavonoids

570    and carotenoids (Figure S2B). Multiple transcripts encoding for peroxidases, dirigent proteins

571    and one laccase were also highly up-regulated in –Fe–P treatment (Table S2). This led to the

572    speculation that dirigent-guided lignin deposition might be up-regulated in the roots during

573    this combinatorial deficiency of Fe and P. Dirigent proteins in plants are well known to

574    modulate cell wall metabolism during abiotic and biotic stress exposure (Paniagua *et al.*,

575    2017). The high cell wall related activity in wheat roots could be correlated with the

576    enhanced root biomass allocation (Figure 1F). Previously it was observed that lignin

577 biosynthesis could be linked with the excess Fe related responses to provide tolerance in rice

578 (Stein *et al.*, 2019). The confirmatory role of lignification needs the functional attention in

579 wheat to address this under dual deficiency. In addition to that Cytochrome P450, a key

580 player in plant development, biotic and abiotic stresses (Narusaka *et al.*, 2004). These gene

581 families are also considered as a scaffold-proteins for the lignin biosynthesis. Based on our

582 analysis, including physiological and biochemical, increased lignification process in the roots

583 during the –Fe–P condition could be one of the important biochemical hallmarks.

584

585 KEGG enrichment analysis reinforced our finding that genes encoding for glutathione

586 metabolism were significantly enriched during –Fe–P treatment. Glutathione levels, its

587 metabolism and activity have been correlated with the tolerance for –Fe (Zaharieva and

588 Abadia, 2003; Bashir *et al.*, 2007; Kaur *et al.*, 2019). The increased burst of glutathione

589 metabolism related genes provide evidence that graminaceous and Eucoids plants under –Fe–

590 P show a very high glutathione related metabolism to compensate for the Fe-deficiency.

591 Other components such as nitric oxide-mediated iron uptake response is also controlled by

592 the supply of glutathione (Shanmugam *et al.*, 2015). The robust expression of glutathione

593 related genes in –Fe–P condition suggest that the plants are undergoing through a strong

594 redox process that is required to survive under combinatorial deficiency. Accumulation of

595 glycine and serine has been implicated to negatively affect root length and nitrate uptake in

596 *Brassica campestris* .Our data from this and previous study for contrasting levels of glycine

597 and serine accumulation could explain the short roots during –Fe compared to +Fe+P, –P and

598 –Fe –P (Kaur *et al.*, 2019). Glycine can induce ethylene guided inhibition of root elongation

599 or it could be converted into amino butyric acid moieties during stress (Han *et al.*, 2018;

600 Igamberdiev and Kleczkowski, 2019).

601

602 In contrast to during Fe-deficiency, we have observed an increase in the root growth

603 and biomass under P-deficiency, which was maintained in response dual deficiency i.e. –Fe–

604 P. Worth to mention that in the model plant, the opposite situation was observed. Short

605 primary root under –P and recovery by –P–Fe (Bouain et al., 2019). This indicate that dicots

606 and monocots have evolved distinct genetic programs to respond to single and/or combined

607 nutrient stress. While most of the studies pertaining to the nutrient interaction have been

608 limited to the vegetative stage, there are limited studies on the molecular basis regulating co-

609 occurring nutrients deficiency during the reproductive stage. Individual nutrient Fe or P stress

610 in crops including wheat affects the overall physiological growth and development; and yield

611    components (Clark *et al.*, 1988; Carstensen *et al.*, 2018).  Our study further confirmed that

612    deficiency of either P or Fe largely impacts plant productivity, with Fe-deficiency causing

613    more impact when compared to P. More importantly, we showed that Fe-deficiency induced

614    morphological changes (i.e. spikelets and roots) that can be restored by removing P from the

615    growth solution. For instance, we revealed that wheat spikelet components support the co-

616    relation for the awn and rachis length to the grain quality (Figure 7C). The drastic reduction

617    in the length of awn, rachis in turn affected the grain yields. In tobacco, it has been proven

618    that inhibiting Fe uptake and transport can induce morphological abnormalities including

619    infertility (Takahashi *et al.*, 2003). The inhibitory effect of –Fe was rescued by the dual

620    deficiency of Fe and P, suggesting the removal of macronutrient such as P could minimize

621    the impact of Fe-deficiency. Also, it is clear that understanding how plants integrate P and Fe

622    signals to controls plant development at reproductive stage is at it is early stage. Our data

623    opens new research avenues to uncover the molecular basis of P and Fe signalling crosstalk

624    in plants, and will lead to designing strategies to develop wheat cultivars with an improved

625    Fe and P use efficiency.

626

634

635    **REFERENCES**

636    **Abadia J, Vazquez S, Rellan-Alvarez R, El-Jendoubi H, Abadia A, Alvarez-Fernandez**

637    **A, Lopez-Millan AF**. 2011. Towards a knowledge-based correction of iron chlorosis. Plant

638    physiology and biochemistry : PPB **49**, 471–482.

639    **Aggarwal S, Kumar A, Bhati KK, Kaur G, Shukla V, Tiwari S, Pandey AK**. 2018.

640    RNAi-Mediated Downregulation of Inositol Pentakisphosphate Kinase (IPK1) in Wheat

641    Grains Decreases Phytic Acid Levels and Increases Fe and Zn Accumulation. Frontiers in

642    plant science **9**, 259.

643    **Aksamit-Stachurska A, Korobczak-Sosna A, Kulma A, Szopa J**. 2008.

644    Glycosyltransferase efficiently controls phenylpropanoid pathway. BMC Biotechnology **8**,

645    25.

646    **Anoop VM, Basu U, McCammon MT, McAlister-Henn L, Taylor GJ**. 2003. Modulation

647    of citrate metabolism alters aluminum tolerance in yeast and transgenic canola

648    overexpressing a mitochondrial citrate synthase. Plant physiology **132**, 2205–2217.

649    **Bashir K, Nagasaka S, Itai RN, Kobayashi T, Takahashi M, Nakanishi H, Mori S,**

650    **Nishizawa NK**. 2007. Expression and enzyme activity of glutathione reductase is

651    upregulated by Fe-deficiency in graminaceous plants. Plant molecular biology **65**, 277–284.

652    **Bhati KK, Alok A, Kumar A, Kaur J, Tiwari S, Pandey AK**. 2016. Silencing of ABCC13

653    transporter in wheat reveals its involvement in grain development, phytic acid accumulation

654    and lateral root formation. Journal of experimental botany **67**, 4379–4389.

655    **Boerjan W, Ralph J, Baucher M**. 2003. Lignin biosynthesis. Annual review of plant

656    biology **54**, 519–546.

657    **Bouain N, Doumas P, Rouached H**. 2016. Recent Advances in Understanding the

658    Molecular Mechanisms Regulating the Root System Response to Phosphate Deficiency in

659    Arabidopsis. Current genomics **17**, 304–308.

660    **Bouain N, Shahzad Z, Rouached A, Khan GA, Berthomieu P, Abdelly C, Poirier Y,**

661    **Rouached H**. 2014. Phosphate and zinc transport and signalling in plants: toward a better

662    understanding of their homeostasis interaction. Journal of Experimental Botany **65**, 5725–

663    5741.

664    **Cai H, Xie W, Zhu T, Lian X**. 2012. Transcriptome response to phosphorus starvation in

665    rice. Acta Physiologiae Plantarum **34**, 327–341.

666    **Carstensen A, Herdean A, Schmidt SB, Sharma A, Spetea C, Pribil M, Husted S**. 2018.

667    The Impacts of Phosphorus Deficiency on the Photosynthetic Electron Transport Chain. Plant

668    Physiology **177**, 271 LP – 284.

669    **Chutia R, Abel S, Ziegler J**. 2019. Iron and Phosphate Deficiency Regulators Concertedly

670    Control Coumarin Profiles in Arabidopsis thaliana Roots During Iron, Phosphate, and

671    Combined Deficiencies   . Frontiers in Plant Science   **10**, 113.

672    **Clark RB, Williams EP, Ross WM, Herron GM, Witt MD**. 1988. Effect of iron deficiency

673    chlorosis on growth and yield component traits of sorghum. Journal of Plant Nutrition **11**,

674    747–754.

675    **Curie C, Panaviene Z, Loulergue C, Dellaporta SL, Briat J-F, Walker EL**. 2001. Maize

676    yellow stripe1 encodes a membrane protein directly involved in Fe(III) uptake. Nature **409**,

677    346–349.

678    **Dalton CC, Iqbal K, Turner DA**. 1983. Iron phosphate precipitation in Murashige and

679    Skoog media. Physiologia Plantarum **57**, 472–476.

680    **Douglas CJ**. 1996. Phenylpropanoid metabolism and lignin biosynthesis: from weeds to

681    trees. Trends in Plant Science **1**, 171–178.

682    **Durrett TP, Gassmann W, Rogers EE**. 2007. The FRD3-Mediated Efflux of Citrate into

683    the Root Vasculature Is Necessary for Efficient Iron Translocation. Plant Physiology **144**,

684    197 LP – 205.

685    **Han R, Khalid M, Juan J, Huang D**. 2018. Exogenous glycine inhibits root elongation and

686    reduces nitrate-N uptake in pak choi (Brassica campestris ssp. Chinensis L.). PLOS ONE **13**,

687    e0204488.

688    **Heuer S, Gaxiola R, Schilling R, Herrera-Estrella L, López-Arredondo D, Wissuwa M,**

689    **Delhaize E, Rouached H**. 2017. Improving phosphorus use efficiency: a complex trait with

690    emerging opportunities. The Plant Journal **90**, 868–885.

691    **Hirsch J, Marin E, Floriani M, Chiarenza S, Richaud P, Nussaume L, Thibaud MC**.

692    2006. Phosphate deficiency promotes modification of iron distribution in Arabidopsis plants.

693    Biochimie **88**, 1767–1771.

694    **Igamberdiev AU, Kleczkowski LA**. 2019. Thermodynamic buffering, stable non-

695    equilibrium and establishment of the computable structure of plant metabolism. Progress in

696    Biophysics and Molecular Biology **146**, 23–36.

697    **Inoue H, Kobayashi T, Nozoye T, Takahashi M, Kakei Y, Suzuki K, Nakazono M,**

698    **Nakanishi H, Mori S, Nishizawa NK**. 2009. Rice OsYSL15 is an iron-regulated iron(III)-

699    deoxymugineic acid transporter expressed in the roots and is essential for iron uptake in early

700    growth of the seedlings. The Journal of biological chemistry **284**, 3470–3479.

701    **Ivanov R, Brumbarova T, Bauer P**. 2012. Fitting into the Harsh Reality: Regulation of

702    Iron-deficiency Responses in Dicotyledonous Plants. Molecular Plant **5**, 27–42.

703    **Kania A, Langlade N, Martinoia E, Neumann G**. 2003. Phosphorus deficiency-induced

704    modifications in citrate catabolism and in cytosolic pH as related to citrate exudation in

705    cluster roots. Plant and Soil **248**, 117–127.

706    **Kaur G, Shukla V, Kumar A,** *et al.* 2019. Integrative analysis of hexaploid wheat roots

707    identifies signature components during iron starvation. Journal of experimental botany **70**,

708    6141–6161.

709    **Kobayashi T, Nishizawa NK**. 2012. Iron uptake, translocation, and regulation in higher

710    plants. Annual review of plant biology **63**, 131–152.

711    **Kumar A, Kaur G, Goel P, Bhati KK, Kaur M, Shukla V, Pandey AK**. 2019. Genome-

712    wide analysis of oligopeptide transporters and detailed characterization of  yellow stripe

713    transporter genes in hexaploid wheat. Functional & integrative genomics **19**, 75–90.

714    **Lee S, Chiecko JC, Kim SA, Walker EL, Lee Y, Guerinot M Lou, An G**. 2009.

715    Disruption of &lt;em&gt;OsYSL15&lt;/em&gt; Leads to Iron Inefficiency in Rice Plants.

716    Plant Physiology **150**, 786 LP – 800.

717    **Ligaba A, Shen H, Shibata K, Yamamoto Y, Tanakamaru S, Matsumoto H**. 2004. The

718    role of phosphorus in aluminium-induced citrate and malate exudation from rape (Brassica

719    napus). Physiologia plantarum **120**, 575–584.

720    **Livak KJ, Schmittgen TD**. 2001. Analysis of relative gene expression data using real-time

721    quantitative PCR and the 2(-Delta Delta C(T)) Method. Methods (San Diego, Calif.) **25**, 402–

722    408.

723    **Love MI, Huber W, Anders S**. 2014. Moderated estimation of fold change and dispersion

724    for RNA-seq data with DESeq2. Genome Biology **15**, 550.

725    **Lucena C, Porras R, García MJ, Alcántara E, Pérez-Vicente R, Zamarreño ÁM,**

726    **Bacaicoa E, García-Mina JM, Smith AP, Romera FJ**. 2019. Ethylene and Phloem Signals

727    Are Involved in the Regulation of Responses to Fe and P Deficiencies in Roots of Strategy I

728    Plants . Frontiers in Plant Science **10**, 1237.

729    **Ma JF, Ling H-Q**. 2009. Iron for plants and humans. Plant and Soil **325**, 1–3.

730    **Marschner H**. 1995. 9 - Functions of Mineral Nutrients: Micronutrients. In: Marschner

731    HBT-MN of HP (Second E, ed. London: Academic Press, 313–404.

732    **Mimmo T, Del Buono D, Terzano R, Tomasi N, Vigani G, Crecchio C, Pinton R, Zocchi**

733    **G, Cesco S**. 2014. Rhizospheric organic compounds in the soil–microorganism–plant system:

734    their role in iron availability. European Journal of Soil Science **65**, 629–642.

735    **Misson J, Raghothama KG, Jain A, *et al.*** 2005. A genome-wide transcriptional analysis

736    using Arabidopsis thaliana Affymetrix gene chips determined plant responses to phosphate

737    deprivation. Proceedings of the National Academy of Sciences of the United States of

738    America **102**, 11934–11939.

739    **Mollier A, Pellerin S**. 1999. Maize root system growth and development as influenced by

740    phosphorus deficiency. Journal of Experimental Botany **50**, 487–497.

741    **Mora-Macías J, Ojeda-Rivera JO, Gutiérrez-Alanís D, Yong-Villalobos L, Oropeza-**

742    **Aburto A, Raya-González J, Jiménez-Domínguez G, Chávez-Calvillo G, Rellán-Álvarez**

743    **R, Herrera-Estrella L**. 2017. Malate-dependent Fe accumulation is a critical checkpoint in

744    the root developmental response to low phosphate. Proceedings of the National Academy of

745    Sciences **114**, E3563 LP-E3572.

746    **Morrissey J, Guerinot M Lou**. 2009. Iron uptake and transport in plants: the good, the bad,

747 and the ionome. Chemical reviews **109**, 4553–4567.

748 **Murata Y, Ma JF, Yamaji N, Ueno D, Nomoto K, Iwashita T**. 2006. A specific transporter

749 for iron(III)–phytosiderophore in barley roots. The Plant Journal **46**, 563–572.

750 **Narayanan, A. Reddy K**. 1982. Effect of phosphorus deficiency on the form of plant root

751 system. Slough, UK□: Commonwealth Agricultural Bureaux, c1982., 412–417.

752 **Narusaka Y, Narusaka M, Seki M, Umezawa T, Ishida J, Nakajima M, Enju A,**

753 **Shinozaki K**. 2004. Crosstalk in the responses to abiotic and biotic stresses in Arabidopsis:

754 analysis of gene expression in cytochrome P450 gene superfamily by cDNA microarray.

755 Plant molecular biology **55**, 327–342.

756 **Naumann C, Müller J, Sakhonwasee S, Wieghaus A, Hause G, Heisters M,**

757 **Bürstenbinder K, Abel S**. 2019. The Local Phosphate Deficiency Response Activates

758 Endoplasmic Reticulum Stress-Dependent Autophagy. Plant Physiology **179**, 460 LP – 476.

759 **Nozoye T, Nagasaka S, Kobayashi T, Takahashi M, Sato Y, Sato Y, Uozumi N,**

760 **Nakanishi H, Nishizawa NK**. 2011. Phytosiderophore efflux transporters are crucial for iron

761 acquisition in graminaceous plants. Journal of Biological Chemistry **286**, 5446–5454.

762 **Oono Y, Kobayashi F, Kawahara Y, Yazawa T, Handa H, Itoh T, Matsumoto T**. 2013.

763 Characterisation of the wheat (Triticum aestivum L.) transcriptome by de novo assembly for

764 the discovery of phosphate starvation-responsive genes: gene expression in Pi-stressed wheat.

765 BMC genomics **14**, 77.

766 **Paniagua C, Bilkova A, Jackson P,** *et al.* 2017. Dirigent proteins in plants: modulating cell

767 wall metabolism during abiotic and biotic stress exposure. Journal of experimental botany **68**,

768 3287–3301.

769 **Quanbeck S, Brachova L, Campbell A,** *et al.* 2012. Metabolomics as a Hypothesis-

770 Generating Functional Genomics Tool for the Annotation of Arabidopsis thaliana Genes of

771 "Unknown Function" . Frontiers in Plant Science **3**, 15.

772 **Raghothama KG**. 1999. PHOSPHATE ACQUISITION. Annual Review of Plant

773 Physiology and Plant Molecular Biology **50**, 665–693.

774 **Ritchie ME, Phipson B, Wu D, Hu Y, Law CW, Shi W, Smyth GK**. 2015. limma powers

775 differential expression analyses for RNA-sequencing and microarray studies. Nucleic acids

776 research **43**, e47–e47.

777 **Römheld V**. 1991. The role of phytosiderophores in acquisition of iron and other

778 micronutrients in graminaceous species: An ecological approach. Plant and Soil **130**, 127–

779 134.

780 **Römheld V, Marschner H**. 1986. Evidence for a specific uptake system for iron

781    phytosiderophores in roots of grasses. Plant physiology **80**, 175–180.

782    **Rouached H, Arpat AB, Poirier Y**. 2010. Regulation of phosphate starvation responses in

783    plants: signaling players and cross-talks. Molecular plant **3**, 288–299.

784    **Schwarz B, Azodi CB, Shiu S-H, Bauer P**. 2020. Putative cis-Regulatory Elements Predict

785    Iron Deficiency Responses in Arabidopsis Roots. Plant Physiology **182**, 1420 LP – 1439.

786    **Secco D, Bouain N, Rouached A, Prom-U-Thai C, Hanin M, Pandey AK, Rouached H**.

787    2017. Phosphate, phytate and phytases in plants: from fundamental knowledge gained in

788    Arabidopsis to potential biotechnological applications in wheat. Critical reviews in

789    biotechnology **37**, 898–910.

790    **Secco D, Jabnoune M, Walker H, Shou H, Wu P, Poirier Y, Whelan J**. 2013. Spatio-

791    temporal transcript profiling of rice roots and shoots in response to phosphate starvation and

792    recovery. The Plant cell **25**, 4285–4304.

793    **Shanmugam V, Wang Y-W, Tsednee M, Karunakaran K, Yeh K-C**. 2015. Glutathione

794    plays an essential role in nitric oxide-mediated iron-deficiency signaling and iron-deficiency

795    tolerance in Arabidopsis. The Plant Journal **84**, 464–477.

796    **Shimizu A, Yanagihara S, Kawasaki S, Ikehashi H**. 2004. Phosphorus deficiency-induced

797    root elongation and its QTL in rice (Oryza sativa L.). Theoretical and Applied Genetics **109**,

798    1361–1368.

799    **Soneson C, Love MI, Robinson MD**. 2015. Differential analyses for RNA-seq: transcript-

800    level estimates improve gene-level inferences. F1000Research **4**, 1521.

801    **Stein RJ, Duarte GL, Scheunemann L, Spohr MG, de Araújo Júnior AT,**

802    **Ricachenevsky FK, Rosa LMG, Zanchin NIT, Santos RP dos, Fett JP**. 2019. Genotype

803    variation in rice (Oryza sativa l.) tolerance to fe toxicity might be linked to root cell wall

804    lignification. Frontiers in Plant Science **10**, 1–20.

805    **Svistoonoff S, Creff A, Reymond M, Sigoillot-Claude C, Ricaud L, Blanchet A,**

806    **Nussaume L, Desnos T**. 2007. Root tip contact with low-phosphate media reprograms plant

807    root architecture. Nature Genetics **39**, 792–796.

808    **Takagi S**. 1976. Naturally occurring iron-chelating compounds in oat- and rice-root

809    washings. Soil Science and Plant Nutrition **22**, 423–433.

810    **Takahashi M, Terada Y, Nakai I, Nakanishi H, Yoshimura E, Mori S, Nishizawa NK**.

811    2003. Role of nicotianamine in the intracellular delivery of metals and plant reproductive

812    development. The Plant cell **15**, 1263–1280.

813    **Thimm O, Bläsing O, Gibon Y, Nagel A, Meyer S, Krüger P, Selbig J, Müller LA, Rhee**

814    **SY, Stitt M**. 2004. mapman: a user-driven tool to display genomics data sets onto diagrams

815    of metabolic pathways and other biological processes. The Plant Journal **37**, 914–939.

816    **Valentinuzzi F, Pii Y, Vigani G, Lehmann M, Cesco S, Mimmo T**. 2015. Phosphorus and

817    iron deficiencies induce a metabolic reprogramming and affect the exudation traits of the

818    woody plant Fragaria×ananassa. Journal of Experimental Botany **66**, 6483–6495.

819    **Wang Y-H, Garvin DF, Kochian L V**. 2002. Rapid induction of regulatory and transporter

820    genes in response to phosphorus, potassium, and iron deficiencies in tomato roots. Evidence

821    for cross talk and root/rhizosphere-mediated signals. Plant physiology **130**, 1361–1370.

822    **Ward JT, Lahner B, Yakubova E, Salt DE, Raghothama KG**. 2008*a*. The effect of iron

823    on the primary root elongation of Arabidopsis during phosphate deficiency. Plant Physiology

824    **147**, 1181–1191.

825    **Ward JT, Lahner B, Yakubova E, Salt DE, Raghothama KG**. 2008*b*. The effect of iron

826    on the primary root elongation of Arabidopsis during phosphate deficiency. Plant physiology

827    **147**, 1181–1191.

828    **Wickham H**. 2017. Book review: ggplot2 – Elegant Graphics for Data Analysis (2nd

829    Edition). , 2–5.

830    **Wu X, Liu G, Riaz M, Yan L, Jiang C**. 2019. Metabolic changes in roots of trifoliate

831    orange [Poncirus trifoliate (L.) Raf.] as induced by different treatments of boron deficiency

832    and resupply. Plant and Soil **434**, 217–229.

833    **Xie X, Hu W, Fan X, Chen H, Tang M**. 2019. Interactions Between Phosphorus, Zinc, and

834    Iron Homeostasis in Nonmycorrhizal and Mycorrhizal Plants. Frontiers in plant science **10**,

835    1172.

836    **Zaharieva TB, Abadia J**. 2003. Iron deficiency enhances the levels of ascorbate,

837    glutathione, and related enzymes in sugar beet roots. Protoplasma **221**, 269–275.

838    **Zhang F, Sun Y, Pei W,** *et al.* 2015. Involvement of OsPht1;4 in phosphate acquisition and

839    mobilization facilitates embryo development in rice. The Plant journal : for cell and

840    molecular biology **82**, 556–569.

841    **Zhou Y, Neuhäuser B, Neumann G, Ludewig U**. 2020. LaALMT1 mediates malate release

842    from phosphorus-deficient white lupin root tips and metal root to shoot translocation. Plant,

843    Cell & Environment **n/a**.

844    **Zhu A, Ibrahim JG, Love MI**. 2018. Heavy-tailed prior distributions for sequence count

845    data: removing the noise and preserving large differences. Bioinformatics **35**, 2084–2092.

846

847

848

849 **Table 1:** Percentage distribution of top twenty putative frequent cis-regulatory elements

850 (freq-pCREs) analyzed in the RNAseq data (–Fe+P, +Fe–P, –Fe–P) and in shortlisted genes

851 involved during Fe-starvation response (FSR-93 genes) and phosphate starvation response

852 (PSR-50 genes). Detailed list of freq-pCREs analysis is shown in Table S11.

| pCREs (motifs) | Percentage distribution of freq-pCREs in given condition | | | | | Top TF family |
|---|---|---|---|---|---|---|
| | -Fe+P | +Fe-P | -Fe-P | FSR | PSR | |
| CATGCA | 63.82 | 62.22 | 65.79 | **80.65** | 80.00 | ABI3VP1 |
| ATGCAT | 64.20 | 64.68 | 65.72 | **76.34** | 70.00 | B3 |
| GCATGA | 46.09 | 44.41 | 46.91 | **68.82** | 60.00 | B3 |
| ATATAT | 65.87 | 66.42 | 67.52 | **66.67** | 70.00 | ARID |
| AAACTA | 49.29 | 50.49 | 50.65 | **59.14** | 66.00 | ARID |
| TATGCA | 45.24 | 46.50 | 47.05 | **58.06** | 50.00 | ABI3VP1 |
| AATTAA | 54.52 | 55.30 | 54.21 | **54.84** | 56.00 | Homeobox |
| AAAGTA | 42.53 | 43.28 | 41.33 | **53.76** | 32.00 | C2C2-Dof |
| ACTAGT | 43.24 | 41.80 | 41.73 | **50.54** | 32.00 | bHLH |
| AATATG | 49.27 | 49.64 | 48.02 | **49.46** | 52.00 | G2-like |
| CACACG | 43.24 | 42.03 | 42.95 | **49.46** | 28.00 | BZR |
| TAATTA | 48.02 | 50.36 | 49.60 | **47.31** | 54.00 | Homeobox |
| AGCATG | 44.21 | 44.65 | 45.07 | **46.24** | 52.00 | B3 |
| AGGCAT | 33.58 | 34.35 | 33.71 | **45.16** | 38.00 | G2-like |
| AATTGC | 37.12 | 39.23 | 36.29 | **44.09** | 26.00 | Homeobox |
| CCGGCC | 50.82 | 49.48 | 50.40 | **44.09** | 58.00 | GeBP |
| CGGCCG | 48.59 | 47.03 | 46.15 | **44.09** | 54.00 | GeBP |
| AGTCAA | 38.93 | 38.39 | 40.00 | **41.94** | 58.00 | WRKY |
| CGTGCC | 35.68 | 33.08 | 34.78 | **41.94** | 30.00 | bHLH |
| ACGAAA | 37.00 | 36.46 | 37.16 | **40.86** | 28.00 | NLP |

853

854

855

856

857

858

859

860

861

862

863

864

865

866 **LEGENDS FOR FIGURES:**

867 **Figure 1: Effect of Fe and P on the growth of roots and shoots of wheat seedlings**

868 **exposed to the mentioned condition for the period of 5, 10 and 20 days.** (A) Experimental

869 setup and the overall growth of wheat seedlings in the given conditions. Morphology of the

870 wheat seedlings subjected to mentioned stress condition (+Fe+P, +Fe–P, –Fe+P and –Fe-P).

871 Pictures were taken after 5, 10, 20 days. (B) Representative root phenotype of wheat roots

872 after 20 days of treatment. (C) Primary root length of wheat seedlings under treated

873 conditions. (D) Total number of $1^{st}$ order lateral roots and (E) Average total length of lateral

874 roots (n=8). (F) Fresh biomass of the root and shoots of the seedlings (S-shoots; R-roots). #

875 and * indicates significant difference at $p<0.05$ and $p<0.01$ respectively.

876 **Figure 2**: **Effect of Fe and P interaction on metal accumulation and its mobilization.** (A)

877 Phosphate uptake in the seedlings of wheat under different regimes of Fe and P. (B) Metal

878 concentration in roots and shoots of wheat seedling subjected to –Fe, –Pi and –Fe–Pi stress.

879 (C) Phenotype of wheat root seedlings during the combinatorial effects of Fe and P as

880 observed by the Perl's Stain for iron plaque (blue plaques). (D) Estimation of the

881 phytosiderophore release by the wheat roots under the mentioned condition. # and * indicates

882 significant difference at $p<0.05$ and $p<0.01$ respectively.

883 **Figure 3: Transcriptome analysis of wheat roots grown under single (-P, -Fe) and dual**

884 **(-Fe-P) conditions.** (A) Genes differentially expressed in response to different deficiency

885 conditions (Dual, -Fe-P; P deficiency, +Fe–P; Fe deficiency, –Fe+P) w.r.t. Control wheat

886 roots. (B) Venn diagram representing the number of unique as well as common differentially

887 regulated genes for the three conditions w.r.t. Control. (C) Analysis of highest differentially

888 responsive genes during –Fe–P condition. Increasing intensities of red and blue colors

889 represent up- and downregulation, as depicted by the color scale.

890 **Figure 4: Fe deficiencyresponsive transcripts affected by different regimes of P.** (A)

891 Heatmap analysis of 60 genes involved in the auxin biosynthesis and response during –P, –Fe

892 and –Fe –P. (B) Analysis of PSR related genes during Fe deficiency (-Fe) and combinatorial

893 deficiency –Fe–P. In total 50 PSR related DEGs belonging to the category of uptake,

894 transport and regulation were used for the analysis. (C) Effect of additional P deficiency on

895 Fe responsive genes. Inner circle of the sunburst graph represents transcripts up- and

896 downregulated under Fe stress while outer concentric circle represents the distribution of said

897 these genes upon dual combined stress. (UP: upregulated; Down: Downregulated; Dual_no:

898 not DE under –Fe–P). (D) Heatmap analysis of 93 iron responsive DEGs involved in Fe

899 uptake, mobilization and regulation (identified from Kaur et al., 2019) during –P and –Fe –P.

27

900    **Figure 5: Mapman and KEGG Pathway enrichment analysis.** (A) Detailed analysis of

901    DEGs for UDP glycosyltransferases, cytochrome P450 and Glutathione-S-transferases. Log2

902    fold change values of the DEGs were imported into MapMan. Red and blue bins represent

903    up-regulation and down-regulation as shown by the scale. (B) Significantly enriched

904    pathways (qvalue< 0.05) for +Fe –P (P-deficiency) and  –Fe –P (dual) deficiency. X-axis

905    depicts the rich-factor, i.e., the ratio of perturbed genes in a pathway w.r.t. the total number of

906    genes involved in the respective pathway, y-axis represents the enriched pathway names,

907    bubble sizes depict the number of genes altered in respective pathways, and increasing

908    intensity of blue color represents increasing significance (decreasing q-value).

909    **Figure 6: Overview of the changes in metabolome in roots of wheat seedlings subjected**

910    **to different growth regimes of Fe and P.** (A) Heatmap distribution of the different

911    metabolome (GC-MS) analysis in the respective replicates of each conditions for of the

912    metabolites. Individual metabolites are expressed in terms of concentrations (µg/mg, fresh

913    weight). Data are means ±SD of n=3 experiments. Metabolites are sorted according to their

914    classes specifically, Sugars, general acids, amino acids, sugar conjugates, fatty acids and

915    polyols. (B) Quantitative plot for the metabolite concentrations (µg/mg FW) for response

916    specific to –Fe –P and response common in –Fe and –Fe–P. Different symbols indicate

917    significant differences between the conditions as determined by Fisher's LSD ($p < 0.05$). +Fe

918    +P, control; -Fe +P, Fe deficiency; +Fe –P, P deficiency; –Fe –P, Fe and P deficiency. 'a'

919    represent significant difference against control, '#' represent significant difference against Fe

920    deficiency and '@' represent significant difference against P deficiency. Red and green bins

921    represent up-regulation and down-regulation with Log2 fold change values as shown by the

922    scale.

923    **Figure 7: Phenotype of wheat grown under different Fe/P concentrations.** (A)

924    Phenotypic representation of wheat plants subjected to multiple treatments (after 45 days of

925    treatments). (B) Spike length for the respective treatments (n=5). (C) Phenotypic

926    characteristics of different tissue of the spike (glumes, rachis, awn and seeds). (D) Averaged

927    weight of mentioned tissue normalized to per spike. The represented values are calculated

928    from biological replicates with 5 replicates (spikes)for each tissue.

929

930    **LEGEND FOR SUPPLEMENTARY DATA**

931

932    **Figure S1: Expression correlation within replicates and across distinct conditions from**

933    **RNAseq data.** A) Principal component analysis (PCA) and B) Cluster heatmap analysis of

934 genes across different deficiency conditions (+Fe-P, –Fe+P and –Fe–P) and control (+Fe+P)

935 for a period of 20 days in wheat roots. Genes with highest variation across these four

936 conditions were used for generating the heatmap using pheatmap package. The change from

937 blue to red color in the color scale depicts increasing gene expression.

938 **Figure S2: MapMan based functional enrichment analysis.** A) Hormone biosynthesis and

939 regulation related perturbed genes in -P (left pane) and -Fe-P (right pane) represented as bins

940 for the respective hormones. B) Secondary metabolism related genes altered in –Fe–P

941 condition. Log2FC values for the respective conditions w.r.t. control was used as input for

942 MapMan, Red and blue colored bins represent up and downregulation of genes, as depicted

943 by the scale.

944 **Figure S3: qRT-PCR analysis of genes involved in Fe uptake/mobilization.** Total of 2 μg

945 of RNA was used for cDNA synthesis and qRT-PCR was performed using gene specific

946 primers (Table S1). $C_t$ values were normalized against wheat *ARF1* as an internal control.

947 **Figure S4: MapMan metabolism overview for the DEGs in P and Fe** deficiency**.**

948 Metabolism overview demonstrating differentially expressed transcripts involved in different

949 functional categories, under A) –P and B) –Fe–P deficiency samples w.r.t. control wheat

950 roots. Log2FC values for the respective conditions w.r.t. control was used as input for

951 MapMan, red and blue colored bins represent up and downregulation of genes.

952 **Figure S5: MapMan visualization depicting the differentially expressed transcription**

953 **factors families (TFs) for –P (top) and –Fe-P (bottom) conditions w.r.t. Control wheat**

954 **roots.** The red and blue coloured bins represent up and down-regulated transcripts. Numbers

955 in the scale represent fold changes in expression levels expressed as Log2.

956

957 **Table S1: Primers used in the current study.**

958 **Table S2: DEGs in response to Fe and P deficiency in wheat roots.** List of upregulated

959 genes and downregulated genes (multiple sheets) in respective conditions. Tables enlists

960 genes perturbed during –P (upregulated and downregulated) and –Fe–P (upregulated and

961 down regulated) with reference to the control samples. Our older RNAseq (Kaur et. al., 2019,

962 BioProjectID-PRJNA529036) analysis was also repeated using Kallisto-DESeq2 pipeline,

963 and thus -Fe (up-regulated and downregulated) perturbed genes are also listed in different

964 sheets. DEGs were annotated with information like gene description, rice ortholog, ortholog

965 based gene definition, KEGG Orthology, Pathways and Pfam domains, which were obtained

966    through KOBAS 3.0 stand-alone tool, using Oryza sativa RAP-DB as reference and also

967    using wheat RefSeq v1.1.

968    **Table S3: Unique genes within DEGs in response to Fe and/or P deficiencyw.r.t. control**

969    **in wheat roots.** List of unique DEGs expressed during each respective condition, –P, –Fe and

970    –Fe–P (upregulated and down regulated).

971    **Table S4: Common genes among the DEGs in response to Fe and/or P deficiency w.r.t.**

972    **control in wheat roots, as displayed in the Venn diagram.** List of common genes regulated

973    by –P and –Fe–P (Sheet1), –Fe and –Fe–P (Sheet2), –Fe and –P (Sheet3). Genes regulated

974    commonly either in same or opposite direction have been included. (NC: No significant

975    change in expression)

976    **Table S5: List of DEGs encoding for different transcription factors those are**

977    **differentially up- and downregulated.** MapMan was used to identify TFs and categorize

978    them into TF families. Table gives logFC value for deficiency vs control under –P, -Fe and –

979    Fe–P conditions. A gradient of red and green is used for upregulated and downregulated TFs

980    respectively.

981    **Table S6: List of Auxin homeostasis related genes.** Genes involved in Auxin biosynthesis

982    were shortlisted using orthologs from rice obtained using KOBAS annotation tool, while

983    other genes involved in degradation, signal transduction and auxin responsive genes were

984    identified using MapMan.

985    **Table S7: List of Phosphate deficiency responsive and Fe stress responsive genes.** Genes

986    central to the uptake, transport and regulation for P and Fe under the respective stresses were

987    shortlisted.

988    **Table S8: Common and contrasting genes specific for –P and –Fe–P.** Lists for 39 genes

989    upregulated in both –P and –Fe–P; 96 genes downregulated in both –P and –Fe–P; 146 genes

990    that are oppositely regulated in –P and –Fe–P.

991    **Table S9: Common and contrasting genes specific for -Fe and -Fe-P.** Lists Fe altered

992    genes that were still differentially responsive in additional absence of P, either showing the

993    same (410 genes; 356 upregulated in both conditions, 54 downregulated in both) or

994    contrasting pattern of expression (200 genes). Also listed are 84 genes commonly regulated

995    in all 3 conditions.

996    **Table S10:** GC-MS analysis of wheat roots subjected to different regimes of Fe and P. Each

997    metabolite is represented with concentrations in three independent replicate manners. For

998    concentration calculation, individual metabolite area was normalized to sample weight and

999    area of internal control (sorbitol). Metabolites with no detectable area in any of the conditions

1000    were considered to be the metabolite with minimum area. Delta method approximation was

1001    used to calculate standard errors (se) of log-ratio, se log-ratio = $1/\ln 2\sqrt{[(SET/T)2 + (SEC}$

1002    /C)2 ], where SET and SEC are standard errors of average +Fe -P/-P +Fe/-Fe -P and +Fe +P

1003    metabolite abundances, respectively. Metabolites with significant (p-value <0.05) differential

1004    abundance were plotted.

1005    **Table S11: Percentage distribution of frequent putative cis-regulatory elements (freq-**

1006    **pCREs) analysed in RNASeq data.** DEGs from the three deficiency conditions were

1007    selected, their promoters were searched for the presence of the 115 freq-pCREs enriched in

1008    Fe GS clusters (Schwarz et al., 2020). Percentage distribution was also analysed for FSR and

1009    PSR genes. For control sample, three sets of 100 genes with no DE under -Fe condition were

1010    randomly selected and analyzed. TF family for respective motifs were obtained from

1011    Schwarz et al., 2020.

1012    **Table S12: Percentage distribution of PHR1 binding site (P1BS) motifs in the promoter**

1013    **region of transcripts DE in RNASeq data and specifically in the genes involved in FSR,**

1014    **PSR genes (Sheet 1).** PSR and FSR genes followed by the number of P1BS motifs found in

1015    each gene's promoter region (Sheet 2 and 3).

1016

(A)



(B)



(C)



(D)



(E)



(F)



Figure 1

(A)



(B)



(C)



(D)
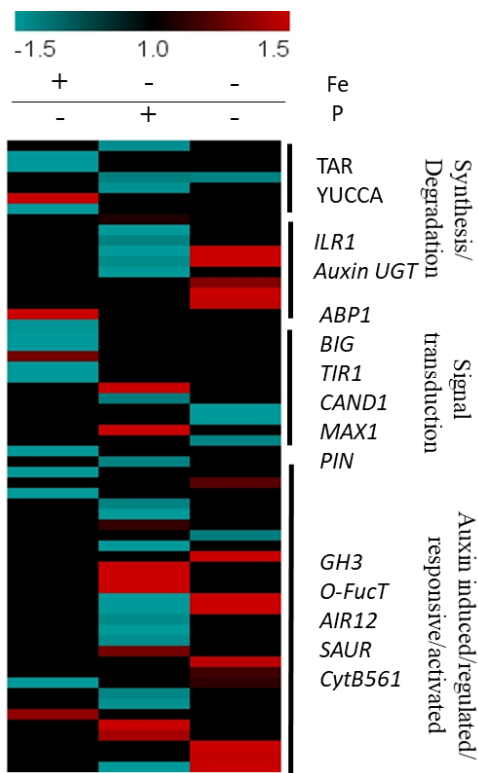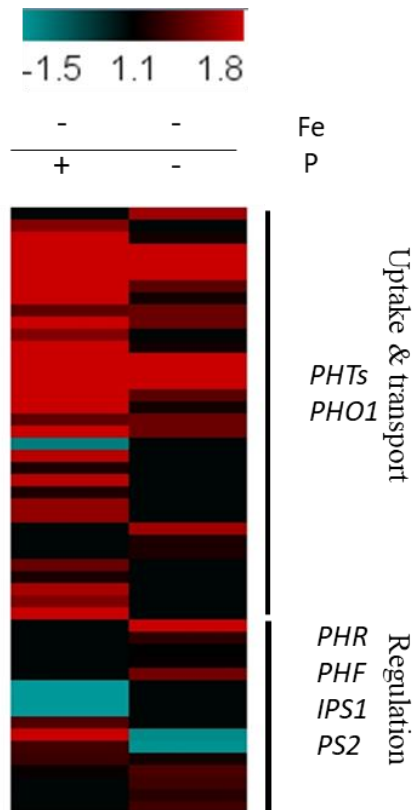


Figure 2

(A)

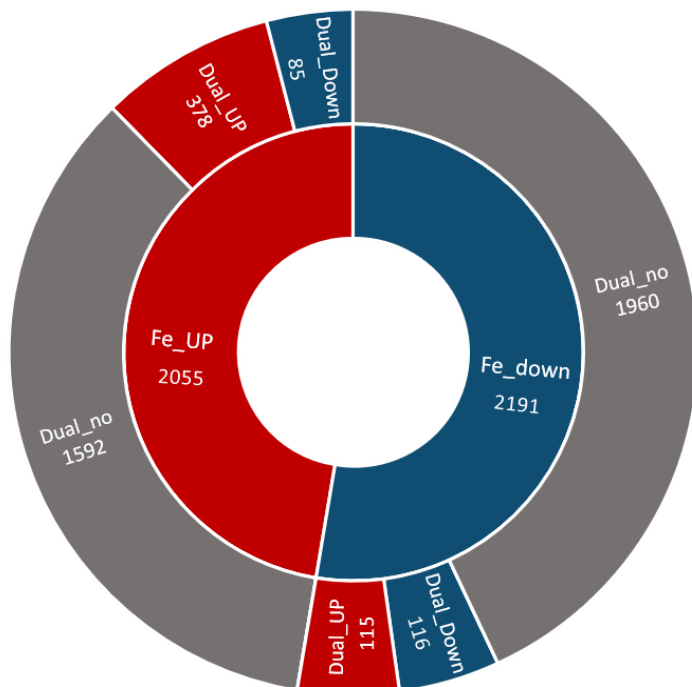Upregulated    Downregulated



(B)



(C)
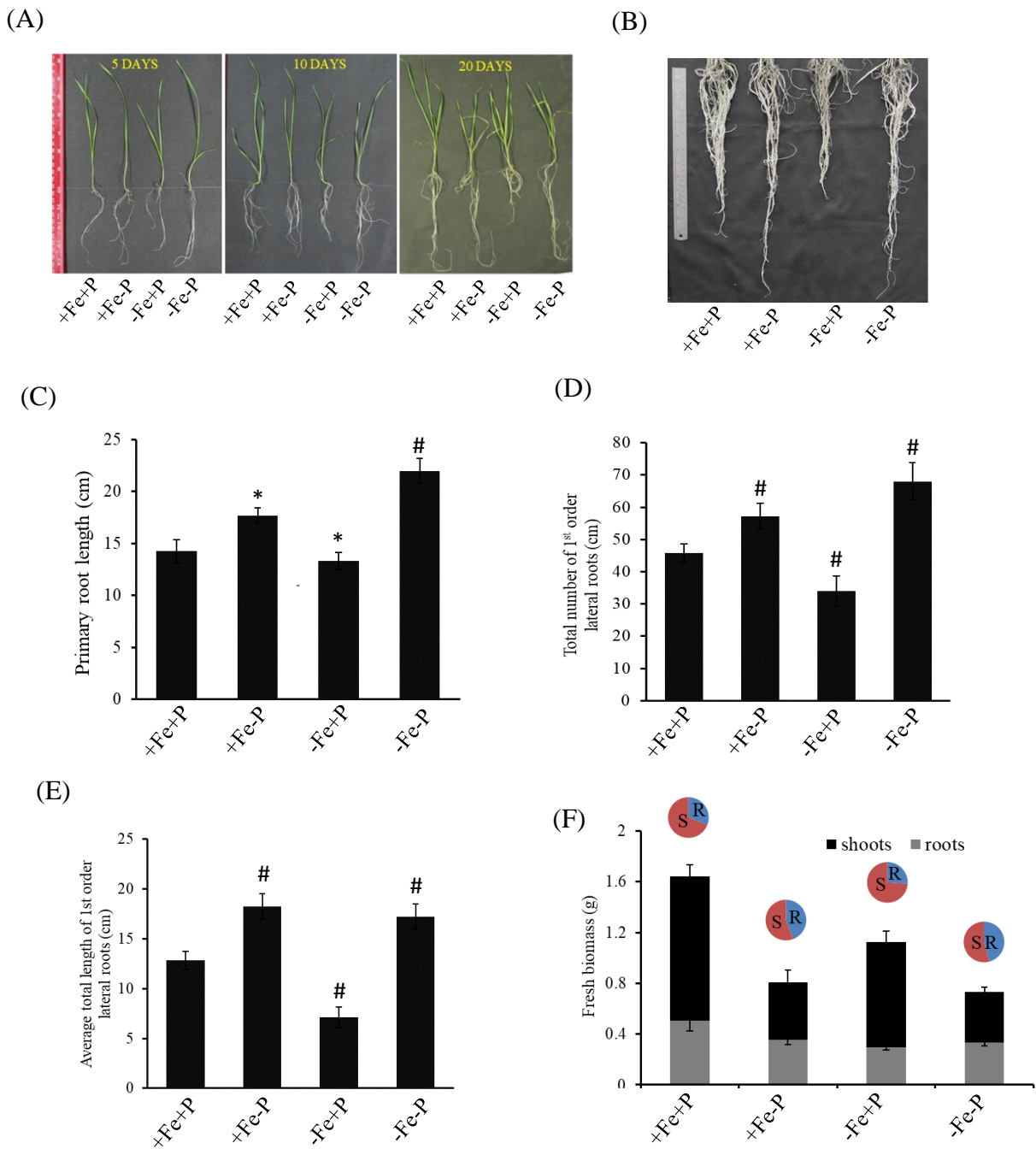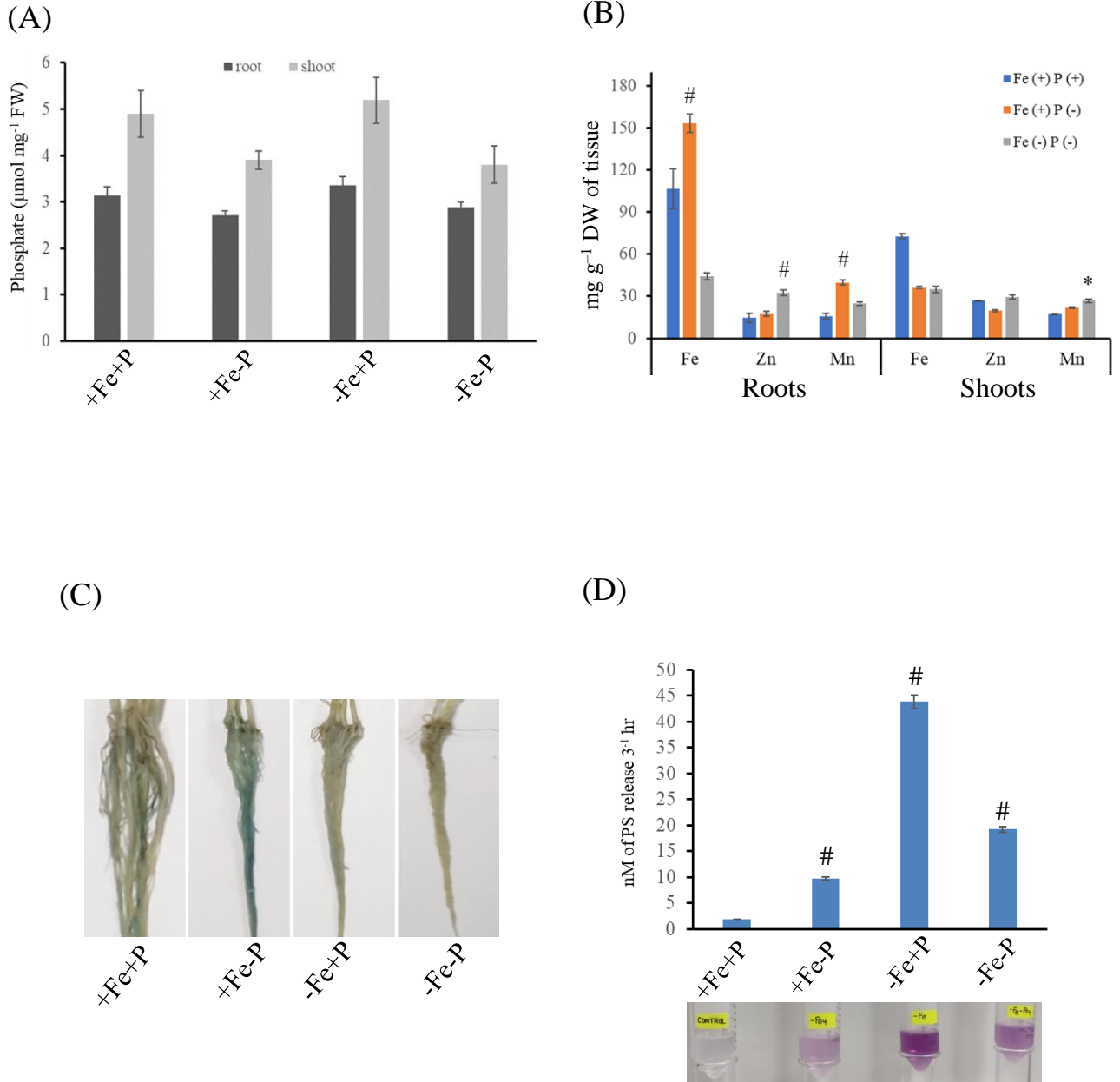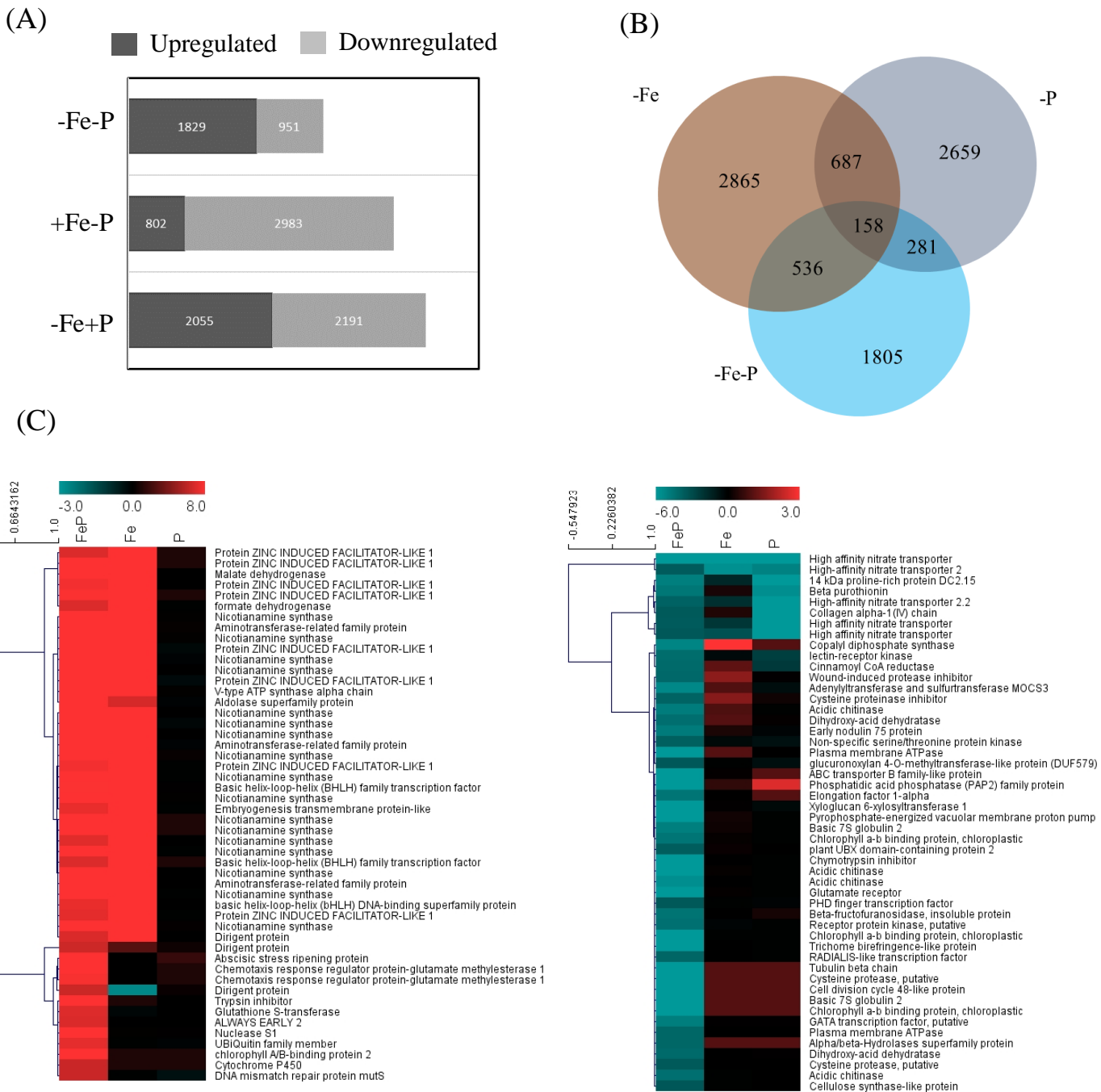


Figure 3

(A)

(B)



(C)

Fe response to +P and -P

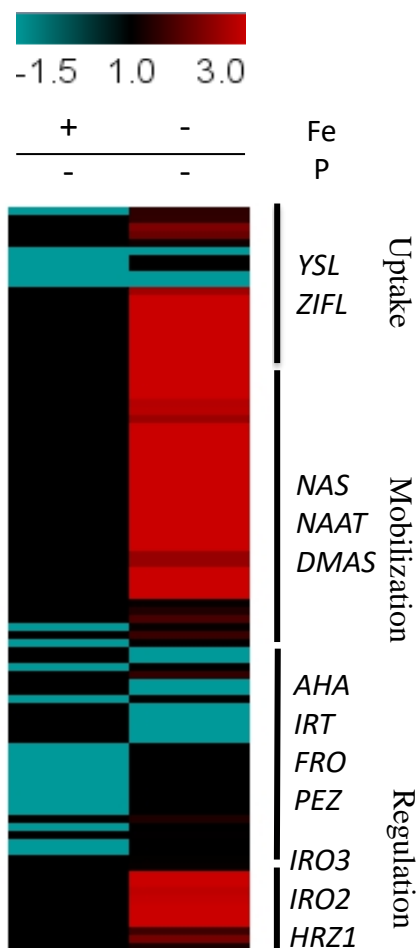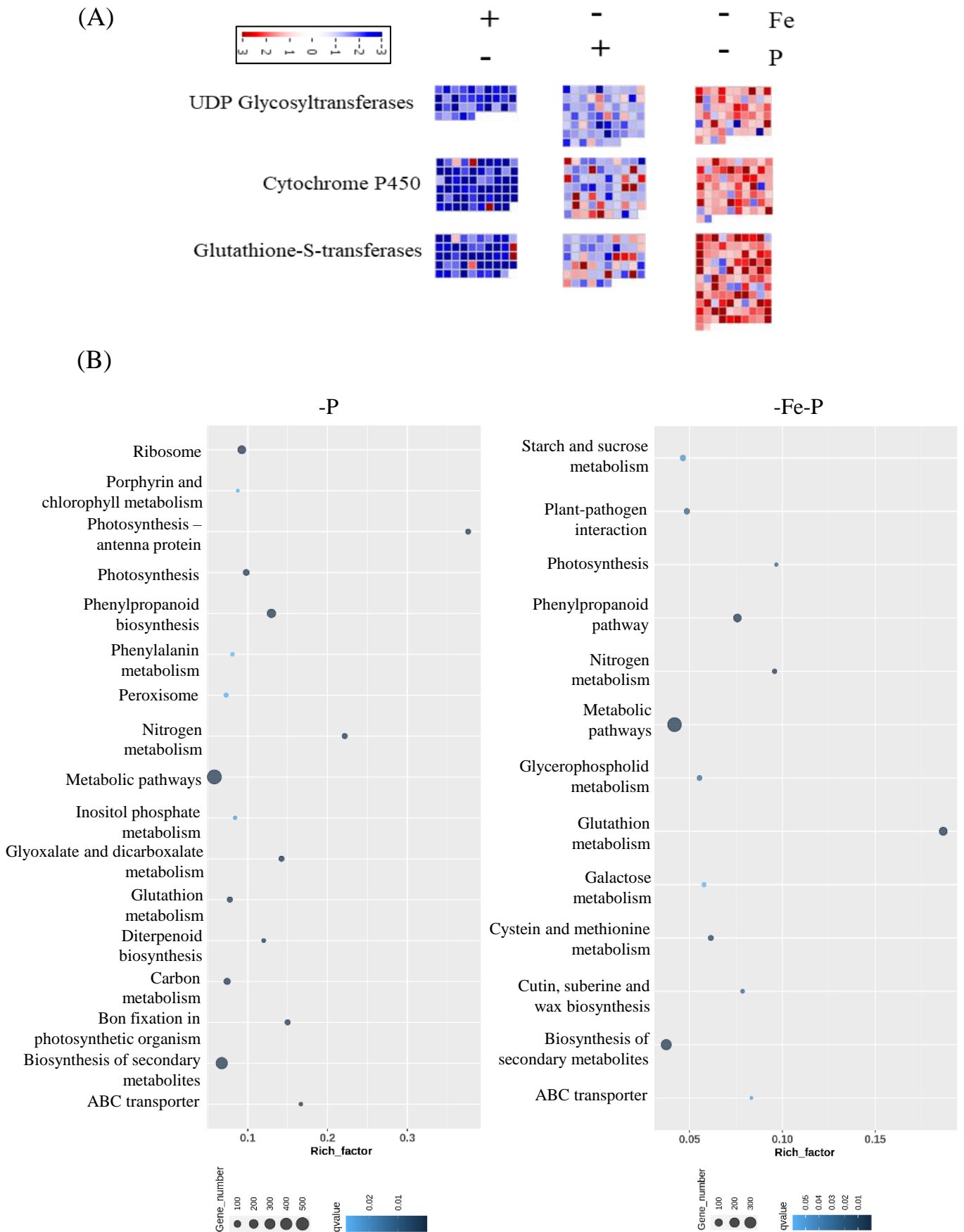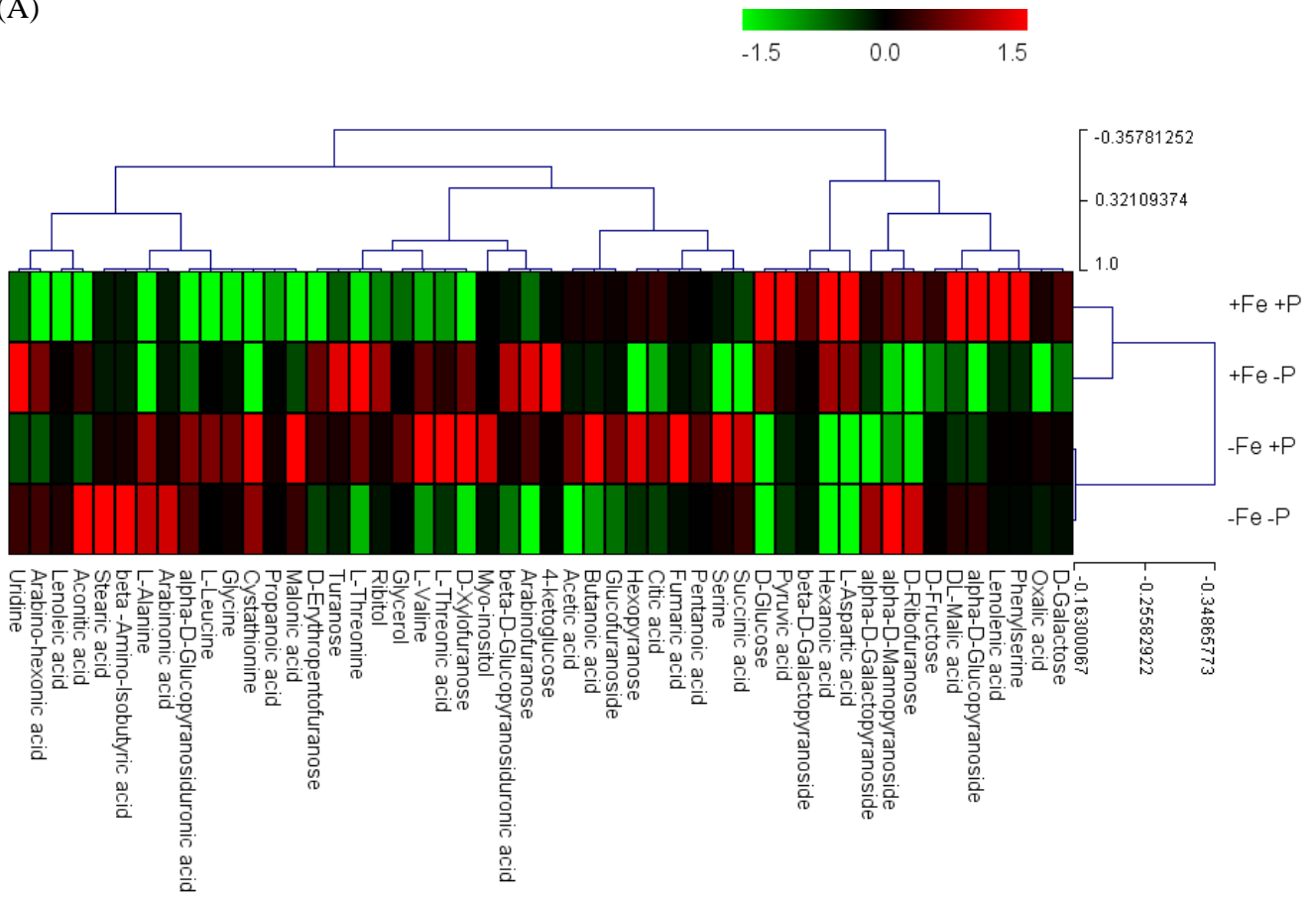

(D)



Figure 4

Figure 5

(A)



(B)



Figure 6

(A)



(B)



(C)



(D)



Figure 7